Enhancing the performance of hybrid wave-wind energy systems through a fast and adaptive chaotic multi-objective swarm optimisation method

Mehdi Neshat [a,b], Nataliia Y. Sergiienko [c], Meysam Majidi Nezhad [e], Leandro S.P. da Silva [f], Erfan Amini [g], Reza Marsooli [g], Davide Astiaso Garcia [d,*], Seyedali Mirjalili [a,h]

[a] *Center for Artificial Intelligence Research and optimisation, Torrens University Australia, Brisbane, QLD, 4006, Australia*
[b] *Faculty of Engineering and Information Technology, University of Technology Sydney, Ultimo, NSW, 2007, Australia*
[c] *School of Electrical and Mechanical Engineering, University of Adelaide, Adelaide, SA, 5005, Australia*
[d] *Department of Planning, Design, and Technology of Architecture, Sapienza University of Rome, Italy*
[e] *Department of Sustainable Energy Systems, Mälardalen University, Västerås, SE 72123, Sweden*
[f] *Delmar Systems, Perth, WA, 6000, Australia*
[g] *Department of Civil, Environmental and Ocean Engineering, Stevens Institute of Technology, Hoboken, NJ, United States*
[h] *University Research and Innovation Center (EKIK), Obuda University, Budapest, 1034, Hungary*

ARTICLE INFO

ABSTRACT

Hybrid offshore renewable energy platforms have been proposed to optimise power production and reduce the levelised cost of energy by integrating or co-locating several renewable technologies. One example is a hybrid wave-wind energy system that combines offshore wind turbines with wave energy converters (WECs) on a single floating foundation. The design of such systems involves multiple parameters and performance measures, making it a complex, multi-modal, and expensive optimisation problem. This paper proposes a novel, robust and effective multi-objective swarm optimisation method (DMOGWA) to provide a design solution that best compromises between maximising WEC power output and minimising the effect on wind turbine nacelle acceleration. The proposed method uses a chaotic adaptive search strategy with a dynamic archive of non-dominated solutions based on diversity to speed up the convergence rate and enhance the Pareto front quality. Furthermore, a modified exploitation technique (Discretisation Strategy) is proposed to handle the large damping and spring coefficient of the Power Take-off (PTO) search space. To evaluate the efficiency of the proposed method, we compare the DMOGWA with four well-known multi-objective swarm intelligence methods (MOPSO, MALO, MODA, and MOGWA) and four popular evolutionary multi-objective algorithms (NSGA-II, MOEA/D, SPEA-II, and PESA-II) based on four potential deployment sites on the South Coast of Australia. The optimisation results demonstrate the dominance of the DMOGWA compared with the other eight methods in terms of convergence speed and quality of solutions proposed. Furthermore, adjusting the hybrid wave-wind model's parameters (WEC design and PTO parameters) using the proposed method (DMOGWA parameters) leads to a considerably improved power output (average proximate boost of 138.5%) and a notable decline in wind turbine nacelle acceleration (41%) throughout the entire operational spectrum compared with the other methods. This improvement could lead to millions of dollars in additional income per year over the lifespan of hybrid offshore renewable energy platforms.

1. Introduction

The growing concerns over climate change and the depletion of fossil fuels have led to an increased focus on the development of renewable energy resources [1,2]. Offshore renewable energy refers to the energy that can be extracted from ocean waves, tides and currents [3], as well as offshore winds [4]. Hybrid renewable energy platforms [5], combining various energy sources, have been increasingly studied as they show promise in improving power output efficiency and reducing the levelised cost of energy [6,7]. Among these systems, a hybrid wave-wind power platform that integrates offshore wind turbines and one or more wave energy converters (WECs) is a promising solution for harnessing the vast energy available in the ocean. [8]. In line with

---

global initiatives, the Net Zero Emission 2050 Plan, as a part of the Paris Agreement, has become a pivotal area of research and action [9]. This ambitious plan aims to achieve net-zero greenhouse gas emissions by 2050 [10], necessitating a profound shift in energy production and consumption patterns [11,12]. In Australia, the pursuit of this target is particularly significant due to the country's high per capita emissions and its vast potential for renewable energy [13]. The Australian government has initiated several strategies, such as incentivising renewable energy development, phasing out coal-fired power plants, and investing in green technologies [14]. These efforts are complemented by research into advanced renewable energy systems [15], like the hybrid wave-wind platforms, which are expected to play a significant role in Australia's energy transformation.

The integration of wave energy converters (WECs) and floating offshore wind turbines (FOWTs) has gained significant attention as a promising approach to harnessing renewable energy from both wind and waves [16]. This hybrid system offers several advantages, including increased energy production, reduced costs, and improved grid stability. However, the design and optimisation of such hybrid systems pose unique challenges due to the complex interactions between the WECs, FOWTs, and the surrounding environment. Several studies have investigated the potential benefits and challenges of hybrid WEC-FOWT systems. For instance, [17] presented a comprehensive review of the state-of-the-art hybrid WEC-FOWT systems, highlighting the key electrical design considerations, control strategies, and performance assessment methods. The authors emphasised the need for further research on the hydrodynamic interactions between the WECs and FOWTs, as well as the development of advanced control algorithms to optimise the overall system performance. Further, in [18], the authors proposed a novel hybrid WEC-FOWT system concept that utilises a floating platform to support both the WECs and FOWTs. The study employed numerical simulations to investigate the hydrodynamic performance of the hybrid system under various wave and wind conditions. The results demonstrated that the hybrid system can effectively capture energy from both waves and wind, with the WECs contributing significantly to the overall power generation. Another study [19] focuses on the optimisation of a hybrid WEC-FOWT system using a multi-objective algorithm. The optimisation improved the hydrodynamic performance of the hybrid system. The results indicated that the optimal design parameters of the system are highly dependent on the specific site conditions as the energy capture efficiency and the stability of the hybrid system improved by adjusting the position of the floating platform to head waves and beam waves. A recent study [20] on the WECs within a hybrid system combined with a floating offshore wind platform found that larger WECs capture more wave energy and reduce the maximum horizontal force and pitch moment on the platform, indicating potential synergies between wave and wind energy utilisation on floating platforms [21]. Kluger et al. [22] further explored the benefits of incorporating wave power into offshore wind farms.

To optimise the total power output of the hybrid platform, several heterogeneous parameters from wind turbines and WECs must be adjusted, making the problem complex, multi-modal, and computationally expensive. In recent years, several optimisation and AI-based techniques [23] have been applied to solve such complex optimisation problems, including particle swarm optimisation (PSO) [24], multi-objective evolutionary algorithms (MOEAs) [25], and swarm-based optimisation method, such as grey wolf optimiser (GWO) [26]. Despite these advances, there is still a need for more robust and effective optimisation algorithms that can efficiently handle the multi-objective nature of the problem while providing high-quality solutions. Several initial research studies examined the production of electrical power from offshore wind turbines and wave energy converters situated together along the California coastline. The study concluded that the integration of wind and wave farms results in decreased variability of power output, which translates to fewer instances of zero power output

and lower overall costs of system integration, as compared to relying on either wind or wave energy alone.

Following some of these pioneering works, several studies have further investigated different hybrid wave-wind energy system configurations and their benefits, including the integration of energy storage systems [27] and the development of control strategies for optimal power take-off (PTO) [28,29]. To address this issue, multi-objective optimisation techniques have been employed [30,31]. PTO systems, consisting of wave energy converters (WECs) and wind turbines (WTs), are designed to capture wave and wind energy simultaneously, thus offering the potential for significant advantages in terms of energy production, cost reduction, and system reliability compared to standalone systems [32]. The system, which converts the mechanical energy from WECs and WTs into electrical power, is a crucial element in such hybrid systems, as its performance directly influences the overall efficiency and output of the system [33]. Consequently, researchers have increasingly focused on the parameters and strategies for optimising the PTO system in hybrid wave-wind energy systems, including the control strategy, damping, and energy storage [34]. Several studies have explored different control strategies to optimise the PTO system, focusing on maximising energy capture while reducing mechanical stresses on WECs and WTs [28]. Reactive control, which adjusts the PTO damping in response to wave excitation forces, has been shown to significantly enhance energy capture [35].

Optimising control parameters of WECs is a crucial aspect of hybrid wave-wind energy systems, as it enables efficient energy conversion from the combined wave and wind resources into usable electrical power. Various optimisation techniques have been employed to solve such complex problems in renewable energy systems, including single-objective and multi-objective methods [36]. Some of the most widely used single-objective optimisation techniques. However, these techniques cannot efficiently handle the multi-objective nature of the hybrid wave-wind energy system optimisation problem, which requires the consideration of multiple conflicting objectives that need multi-objective methods [37]. Most of these methods aim to generate a Pareto-optimal solution set, considering the trade-offs among the objectives. Among them, NSGA-II is one of the most popular MOEAs and has been widely used in renewable energy system optimisation [24]. Another well-known multi-objective optimisation technique is MOPSO, which is an extension of the PSO algorithm and has been applied in various renewable energy applications, such as microgrid optimisation and optimal sizing of hybrid energy systems [38]. MOEP is an evolutionary programming-based multi-objective algorithm that has been applied in various optimisation problems, including the optimal operation of hydropower systems [39]. Lastly, MOGWO is a recently proposed multi-objective optimisation algorithm based on GWO, which has been utilised in the optimisation of hybrid renewable energy systems, among other applications [31].

In response to the growing interest in hybrid wave-wave energy systems, recent studies have provided significant insights into the complexities of these systems. A recent study [40] offered an in-depth analysis of integrated floating wind-wave power generation platforms, emphasising the importance of fully coupled models in operational sea conditions. Building upon that, another study [41] presents a comprehensive numerical investigation of hydrodynamic responses for a semi-submersible wind turbine combined with various layouts of wave energy converters. This research provided critical data on optimising configurations for maximum efficiency. Furthermore, the research on size optimisation of wave energy converters in a floating wind-wave combined power generation platform [42] highlights the significance of dimensional considerations in such hybrid systems. Collectively, these studies illustrate the complex dynamics and optimisation challenges inherent in hybrid wave-wave systems. Acknowledging these insights, our research aims to build upon these foundational works by introducing a multi-objective optimisation approach. This approach is designed to

address the multifaceted nature of hybrid systems, where multiple conflicting objectives must be considered, thereby enhancing the overall efficiency and effectiveness of these renewable energy systems.

Despite the extensive research on hybrid wave-wind energy systems and the use of various optimisation techniques, there are still gaps in achieving robust and effective optimisation solutions for these systems. Most existing optimisation methods suffer from limitations, such as slow convergence speed, premature convergence, or the inability to maintain diversity in the Pareto-optimal solutions [43]. Moreover, The hydrodynamic interactions between the WECs and FOWTs can significantly affect the overall system performance. However, these interactions are often simplified or neglected in existing studies. A detailed analysis of the hydrodynamic interactions is crucial for understanding the system's behaviour and optimising its performance. Therefore, there is a need for a novel and more effective optimisation method that can address these limitations and provide high-quality solutions for the hybrid wave-wind energy system optimisation problem. In order to achieve the goal of maximising the absorbed power of ocean waves and wind in a hybrid model while simultaneously keeping the acceleration of wind turbines at low levels, this paper presents a solution in the form of a fast and efficient multi-objective swarm optimisation method called DMOGWA.

The proposed method aims to identify optimal solutions that strike the best possible balance between all objectives, taking into account various design parameters from both wind turbines and wave energy converters (WECs). The efficiency of the proposed method is evaluated by comparing the results with eight other well-known multi-objective optimisation algorithms, such as multi-objective particle swarm optimisation (MOPSO), Non-dominated Sorting Genetic Algorithm II [24] (NSGA-II), Pareto Envelope-based Selection Algorithm II [44] (PESA-II), Strength Pareto Evolutionary Algorithm II [45] (SPEA-II), Multi-objective Ant Lion Optimiser [46] (MALO), Multi-Objective Dragonfly Algorithm [47] (MODA), Multi-Objective Evolutionary Algorithm based on Decomposition [48] (MOEA/D), Multi-Objective Particle Swarm Optimisation [49] (MOPSO) and Multi-objective Grey Wolf Optimiser [31] (MOGWA) based on four Australian sea sites, Sydney, Port Lincoln, Gippsland, and Cliff Head. The major contributions of this study are as follows.

- A fast and effective hybrid wave-wind energy system optimisation framework is proposed. The study introduces a novel optimisation framework for hybrid wave-wind energy systems that combines a multi-objective swarm intelligence-based method with a chaotic adaptive search strategy. This integration allows for efficient and effective system optimisation, enabling the selection of non-dominated solutions based on diversity through a dynamic archive.
- To confront the limitations of MOGWO's static archive size, we propose an adaptive mechanism that adjusts to the changing circumstances and dynamically modifies the archive's size throughout the optimisation steps. Our approach harnesses specific diversity measures, particularly the crowding distance concept, to govern the adaptive nature of the archive's dimensions.
- A simple exploitation enhancement technique is introduced. The research presents a discretisation search space format to enhance the optimisation process's exploitation phase. This technique aids in achieving a more refined and accurate optimisation of the hybrid wave-wind energy system.
- Furthermore, the study conducts a comprehensive comparative analysis by evaluating the performance of the proposed hybrid wave-wind energy system optimisation framework against nine well-known multi-objective optimisation methods. This rigorous evaluation allows for identifying the strengths and weaknesses of different approaches and provides insights into the superiority of the proposed framework.
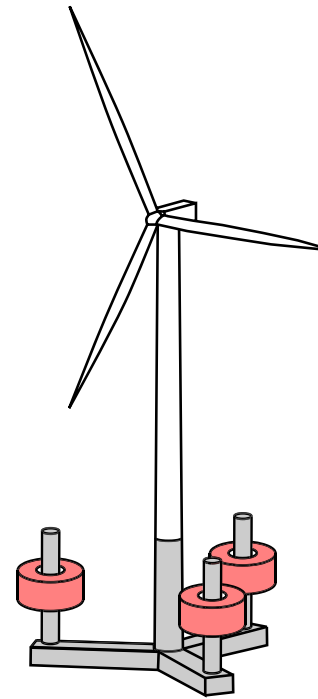

Fig. 1. Hybrid wave-wind system concept.

- Finally, optimisation of hybrid wave-wind systems for four potential deployment sites along the South Coast of Australia. These sites exhibit varying wave characteristics, and the study addresses the site-specific optimisation requirements, ensuring that the proposed framework is adaptable to different sea conditions.

In this paper, we first present the system description and modelling of the hybrid wave-wind system, including equations of motion, deployment site, and performance measures (Section 2). We then describe the optimisation setup (Section 3). Following this, we introduce eight various multi-objective optimisation algorithms and the technical details of the proposed chaotic multi-objective optimisation method in Section 4. Subsequently, we present the numerical results and discussion (Section 5) to compare the efficiency and effectiveness of the proposed method. Finally, we conclude our findings and highlight the advantages of our proposed method.

2. System description and modelling

2.1. Hybrid wave-wind system

The hybrid wave-wind system consists of a braceless semi-submersible platform [50,51] and three torus-shaped WECs attached to the platform's side columns as shown in Fig. 1.

The CSC platform developed by Luan [51] is composed of a central column that is connected to the wind turbine tower, three side columns, and three pontoons with rectangular cross-sections. This platform was designed to support a 5-MW NREL reference wind turbine [52], and its dimensions are specified in Table 1 and Fig. 2. The detailed design of the platform can be found in [51].

Wave energy is extracted from the relative heave motion between the WECs and the platform. It is assumed that the WEC power take-off mechanism acts as a spring-damper system and converts mechanical to electrical power with 100% efficiency. The WEC heave motion is constrained by the physical dimensions of the side columns. The WEC outer diameter and draught are design variables in this study. The inner radius of the WEC is taken as 4.25 m. The platform is assumed to be in 200 m water depth.
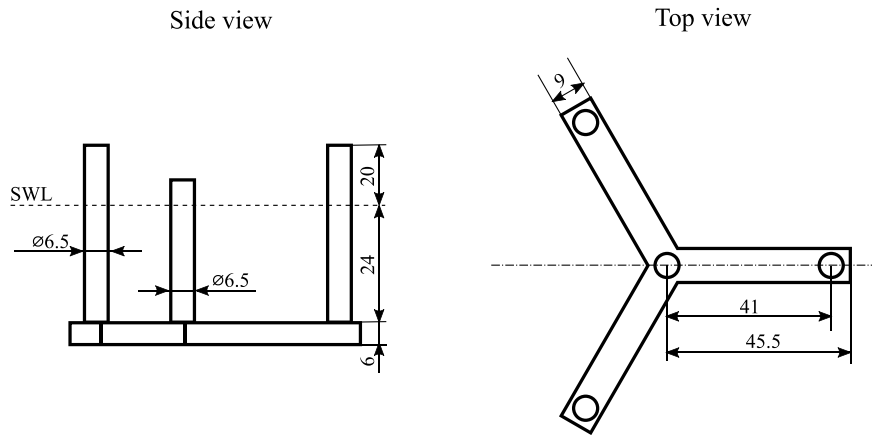
Side view

Top view

Fig. 2. Side and top views of the CSC floating platform.

Table 1
Dimensions of the CSC platform.

Parameter	Value
Central column diameter	6.5 m
Side column diameter	6.5 m
Side column height	44 m
Pontoon height	6 m
Pontoon width	9 m
Distance to side columns	41 m
Operating draft	30 m
Displacement	10,255 t
Steel weight (hull)	1804 t
Equivalent thickness	0.03 m

2.2. Equations of motion

Assuming rigid-body modes and planar motion of the floating platform and three WECs, the wind-wave system has six independent degrees of freedom: two translational modes (surge and heave) and one rotational mode (pitch) for the platform and one translational mode corresponding to the motion of each WEC relative to the platform. A very detailed derivation of the equations of motion for a similar problem can be found in [53]. However, due to the increased number of WECs, the authors took a different approach, in particular, the equations of motion are derived for each body (platform and three WECs) separately, and coupled through the power take-off system and hydrodynamics. In this case, the dynamics of the system are described as:

$$\mathbf{q} = \begin{bmatrix} \mathbf{q}^{fowt} & \mathbf{q}^{wec,1} & \mathbf{q}^{wec,2} & \mathbf{q}^{wec,3} \end{bmatrix}^{\mathrm{T}} \qquad (1)$$

where $\mathbf{q}^{fowt} = [q_1^{fowt} \quad q_3^{fowt} \quad q_5^{fowt}]^{\mathrm{T}}$ is the FOWT's displacement in the surge, heave and pitch with respect to its centre of gravity, $\mathbf{q}^{wec,i} = [q_1^{wec,i} \quad q_3^{wec,i}]^{\mathrm{T}}$ is the displacement of the ith WEC in heave and surge with respect to its centre of gravity. The motion of the ith WEC relative to the floating platform can be written as:

$$q_{rel}^{wec,i} \approx q_3^{wec,i} - q_3^{fowt} + q_5^{fowt} x^{wec,i}, \qquad (2)$$

where $x^{wec,i}$ is the x coordinate of the WEC's centre of gravity.

As a result, the motion of a hybrid system can be described by the following differential equation in the time domain:

$$\mathbf{M}\ddot{\mathbf{q}}(t) = \mathbf{F}_{\mathrm{exc}}(t) + \mathbf{F}_{\mathrm{rad}}(t) + \mathbf{F}_{\mathrm{hs}}(t) + \mathbf{F}_{\mathrm{vd}}(t) + \mathbf{F}_{\mathrm{moor}}(t) + \mathbf{F}_{\mathrm{pto}}(t) + \mathbf{F}_{\mathrm{WT}}(t), \quad (3)$$

where $\mathbf{M} = \mathrm{diag}\left(m^{fowt}, m^{fowt}, I^{fowt}, m_{wec}\mathbf{I}_6\right)$ is the mass matrix of the combined system (platform, tower, RNA, WECs), $\mathbf{F}_{\mathrm{exc}}$ is the wave excitation force, $\mathbf{F}_{\mathrm{rad}}$ is the wave radiation force, $\mathbf{F}_{\mathrm{hs}}$ is the hydrostatic force, $\mathbf{F}_{\mathrm{vd}}$ is the viscous drag force, $\mathbf{F}_{\mathrm{moor}}$ is the forces from mooring lines, $\mathbf{F}_{\mathrm{pto}}$ is the power take-off force, and $\mathbf{F}_{\mathrm{WT}}$ is the force exerted on

the platform from the wind turbine aerodynamic loads. As the main focus is given to the hydrodynamic interaction between the WECs and platform, which are less affected by aerodynamic loads, this model uses a simplified representation of the wind turbine loads based on the steady-state thrust curve, which is represented as a function of the wind velocity, neglecting dynamic effects from the tower, nacelle, rotor, blade pitch angle controller, and drivetrain.

All forces except $\mathbf{F}_{\mathrm{WT}}(t)$ in Eq. (3) have a zero mean value, so the hybrid system response $\mathbf{q}(t)$ can be described in terms of a mean value $\bar{\mathbf{q}}$ and a random zero-mean component $\tilde{\mathbf{q}}$:

$$\mathbf{q}(t) = \bar{\mathbf{q}} + \tilde{\mathbf{q}}(t), \qquad (4)$$

where $\tilde{\mathbf{q}}(t)$ can be expressed using a complex amplitude assuming a sum of harmonic responses of the system $\tilde{\mathbf{q}}(t) = \Re\left\{\sum_{j=1}^{N} \hat{\mathbf{q}}_j \, e^{i\omega_j t + \phi_j}\right\}$, N corresponds to the number of frequencies. As a result, the system response and the forces in Eq. (3) can be written in the frequency domain as:

- radiation force:

$$\hat{\mathbf{F}}_{\mathrm{rad}}(\omega) = -\left(-\omega^2 \mathbf{A}_{\mathrm{rad}}(\omega) + i\omega \mathbf{B}_{\mathrm{rad}}(\omega)\right) \hat{\mathbf{q}}(\omega), \qquad (5)$$

where $\mathbf{A}_{\mathrm{rad}}$ is the radiation-added mass matrix, and $\mathbf{B}_{\mathrm{rad}}$ is the hydrodynamic damping matrix, both matrices include off-diagonal hydrodynamic coupling terms between the platform and WECs, and between WECs;

- the linearised hydrostatic force:

$$\mathbf{F}_{\mathrm{hs}}(t) = -\mathbf{K}_{\mathrm{hs}}\mathbf{q}(t), \qquad (6)$$

or

$$\hat{\mathbf{F}}_{\mathrm{hs}}(\omega) = -\mathbf{K}_{\mathrm{hs}}\hat{\mathbf{q}}(\omega), \qquad (7)$$

where $\mathbf{K}_{\mathrm{hs}}$ is the linear hydrostatic stiffness matrix;

- the nonlinear viscous drag force

$$\mathbf{F}_{\mathrm{vd}}(t) = -\mathbf{B}_{\mathrm{vd}}\dot{\mathbf{q}}(t) \odot |\dot{\mathbf{q}}(t)| \qquad (8)$$

is replaced by an equivalent linear damping term $\mathbf{B}_{\mathrm{eq}}$ by means of statistical linearisation:

$$\hat{\mathbf{F}}_{\mathrm{vd}}(\omega) = -i\omega \mathbf{B}_{\mathrm{eq}}\hat{\mathbf{q}}(\omega), \qquad (9)$$

the approximate viscous drag coefficients for the CSC platform are taken from [51];

- the mooring line loads are linearised as:

$$\mathbf{F}_{\mathrm{moor}} = -\mathbf{K}_{\mathrm{moor}}(\bar{\mathbf{q}})\mathbf{q}, \qquad (10)$$

where the mooring stiffness matrix $\mathbf{K}_{\mathrm{moor}}(\bar{\mathbf{q}})$ is calculated at the mean displaced position $\bar{\mathbf{q}}$;

$$\mathbf{K}_{pto} = \begin{bmatrix} 3K_{pto}^{\infty} & 0 & 3K_{pto}^{\infty}L_z & -K_{pto}^{\infty} & 0 & -K_{pto}^{\infty} & 0 & -K_{pto}^{\infty} & 0 \\ 0 & 3K_{pto} & 0 & 0 & -K_{pto} & 0 & -K_{pto} & 0 & -K_{pto} \\ 3K_{pto}^{\infty}L_z & 0 & \sum_i K_{pto}(x^{wec,i})^2 + 3K_{pto}^{\infty}L_z^2) & -K_{pto}^{\infty}L_z & K_{pto}x^{wec,1} & -K_{pto}^{\infty}L_z & K_{pto}x^{wec,2} & -K_{pto}^{\infty}L_z & K_{pto}x^{wec,3} \\ -K_{pto}^{\infty} & 0 & -K_{pto}^{\infty}L_z & K_{pto}^{\infty} & 0 & 0 & 0 & 0 & 0 \\ 0 & -K_{pto} & K_{pto}x^{wec,1} & 0 & K_{pto} & 0 & 0 & 0 & 0 \\ -K_{pto}^{\infty} & 0 & -K_{pto}^{\infty}L_z & 0 & 0 & K_{pto}^{\infty} & 0 & 0 & 0 \\ 0 & -K_{pto} & K_{pto}x^{wec,2} & 0 & 0 & 0 & K_{pto} & 0 & 0 \\ -K_{pto}^{\infty} & 0 & -K_{pto}^{\infty}L_z & 0 & 0 & 0 & 0 & K_{pto}^{\infty} & 0 \\ 0 & -K_{pto} & K_{pto}x^{wec,3} & 0 & 0 & 0 & 0 & 0 & K_{pto} \end{bmatrix}, \tag{12}$$

Box I.

$$\mathbf{B}_{pto} = \begin{bmatrix} 0 & 0 & 0 & 0 & 0 & 0 & 0 & 0 & 0 \\ 0 & 3B_{pto} & 0 & 0 & -B_{pto} & 0 & -B_{pto} & 0 & -B_{pto} \\ 0 & 0 & \sum_i B_{pto}(x^{wec,i})^2 & 0 & B_{pto}x^{wec,1} & 0 & B_{pto}x^{wec,2} & 0 & B_{pto}x^{wec,3} \\ 0 & 0 & 0 & 0 & 0 & 0 & 0 & 0 & 0 \\ 0 & -B_{pto} & B_{pto}x^{wec,1} & 0 & B_{pto} & 0 & 0 & 0 & 0 \\ 0 & 0 & 0 & 0 & 0 & 0 & 0 & 0 & 0 \\ 0 & -B_{pto} & B_{pto}x^{wec,2} & 0 & 0 & 0 & B_{pto} & 0 & 0 \\ 0 & 0 & 0 & 0 & 0 & 0 & 0 & 0 & 0 \\ 0 & -B_{pto} & B_{pto}x^{wec,3} & 0 & 0 & 0 & 0 & 0 & B_{pto} \end{bmatrix} \tag{13}$$

Box II.

- the PTO forces are:

$$\mathbf{F}_{pto}(t) = -\mathbf{K}_{pto}\mathbf{q}(t) - \mathbf{B}_{pto}\dot{\mathbf{q}}(t), \tag{11}$$

where $\mathbf{K}_{pto}$ and $\mathbf{B}_{pto}$ are the stiffness and damping matrices (see Box I).
setting K_{pto}^{∞} to a large number, the stiffness from the PTO acts as a rigid connection, and the system (platform with three WECs) moves as one body in the surge (see Box II).

- the nonlinear wind turbine loads:

$$\mathbf{F}_{WT} = \begin{bmatrix} 1 & 0 & L_t & \mathbf{0}_{1\times6} \end{bmatrix}^T T_t, \tag{14}$$

where L_t is the vertical distance between the platform's centre of gravity and the hub, and the thrust force T_t is expressed as:

$$T_t = \frac{1}{2}C_T(\lambda, \beta)\rho_a A_t U_r^2, \tag{15}$$

where C_T denotes the aerodynamic thrust coefficient for the mean wind speed that depends on the tip-speed ratio λ and the blade pitch angle β, ρ_a is the air density, $A_t = \pi R^2$ is the swept area of the wind turbine perpendicular to the flow, R is the radius of the wind turbine, and U_r is the relative velocity between the wind speed and wind turbine in the horizontal direction defined as

$$U_r = \bar{U}_w + \tilde{u}_w - \dot{q}_1^{fowt} - \dot{q}_5^{fowt}L_t, \tag{16}$$

$\bar{U}_w$ is the mean wind speed, $\tilde{u}_w$ denotes the zero-mean wind speed fluctuation, L_t is the distance to the nacelle from the SWL. Representing the thrust force using Taylor linearisation as:

$$T_t \approx \bar{T}_t + \frac{\partial T_t}{\partial U_r}\left(U_r - \bar{U}_w\right), \tag{17}$$

where

$$\frac{\partial T_t}{\partial U_r} = \frac{1}{2}\frac{\partial C_T(\lambda, \bar{\beta})}{\partial U_r}\rho_a A_t \bar{U}_w^2 + C_T\left(\bar{\lambda}, \bar{\beta}\right)\rho_a A_t \bar{U}_w, \tag{18}$$

the frequency domain equivalent of the thrust force takes the form:

$$\hat{\mathbf{F}}_{WT}(\omega) = -i\omega \mathbf{B}_{WT}(\bar{U}_w)\hat{\mathbf{q}}(\omega), \tag{19}$$

where the wind turbine damping matrix is:

$$\mathbf{B}_{WT}(\bar{U}_w) = \frac{\partial T_t}{\partial U_r}\begin{bmatrix} \begin{array}{ccc|c} 1 & 0 & L_t & \\ 0 & 0 & 0 & \mathbf{0}_{3\times6} \\ L_t & 0 & L_t^2 & \\ \hline & \mathbf{0}_{6\times3} & & \mathbf{0}_{6\times6} \end{array} \end{bmatrix}. \tag{20}$$

The value of $\frac{\partial T_t}{\partial U_r}$ is calculated based on the thrust and power coefficients of the 5MW-NREL reference wind turbine [52] obtained using a blade element momentum model, where $\bar{\beta}$ and $\bar{\lambda}$ are chosen to maximise the wind turbine power production (Region 2) or to keep the wind turbine rotational speed constant (Region 3).

As a result, Eq. (3) can be written in frequency domain as:

$$\left[-\omega^2(\mathbf{M} + \mathbf{A}_{rad}) + i\omega(\mathbf{B}_{rad} + \mathbf{B}_{eq} + \mathbf{B}_{pto} + \mathbf{B}_{WT}) + \mathbf{K}_{hs} + \mathbf{K}_{moor} + \mathbf{K}_{pto}\right]\hat{\mathbf{q}}$$
$$= \hat{\mathbf{F}}_{exc} + \mathbf{T}\hat{u}_w, \tag{21}$$

where

$$\mathbf{T} = \frac{\partial T_t}{\partial U_r}\begin{bmatrix} 1 & 0 & L_t & \mathbf{0}_{1\times6} \end{bmatrix}^T. \tag{22}$$

In Eq. (21), $\mathbf{A}_{rad}(\omega)$, $\mathbf{B}_{rad}(\omega)$, $\mathbf{K}_{hs}$ and $\hat{\mathbf{F}}_{exc}(\omega)$ are calculated using WAMIT [54] (an example geometry and mesh are shown in Fig. 3), $\mathbf{B}_{eq}$ is estimated using the statistical linearisation technique [55], $\mathbf{B}_{WT}$ and the corresponding $\frac{\partial T_t}{\partial U_r}$ are calculated based on the wind turbine $C_T(\lambda, \beta)$ matrix obtained from AeroDyn [56], and $\mathbf{K}_{moor}$ is taken from [51]. The model is built using MATLAB.

Irregular waves are generated using the JONSWAP spectrum [57] with a peak enhancement factor of 3.3, and the wind spectrum is generated using the Kaimal model [58] with a turbulence level of $I_u \approx 0.12$ at 15 m/s (IEC class C), representative of offshore locations [59]. To take into account the wind speed fluctuations over the swept area of the wind turbine, the aerodynamic admittance function χ^2 [60–62] is used to modify the wind spectrum:

$$\chi^2(\omega) = \left[\frac{1}{1 + \left(\omega\sqrt{A_t}/(\pi\bar{U}_w)\right)^{4/3}}\right]^2. \tag{23}$$
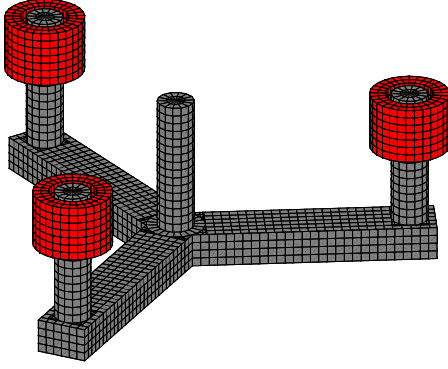
Fig. 3. WAMIT mesh (only submerged part): grey panels correspond to the CSC semi-submersible platform, and red panels correspond to torus-type WECs.

2.3. Site locations and environmental data

The hybrid wave-wind system is optimised for four potential deployment sites on the South Coast of Australia. Fig. 4 shows their approximate locations. The characteristics of four sites and statistical environmental data for the period between 2014 and 2020 are shown in Sections 2.3.1–2.3.4 based on data from the Australian Marine Energy Atlas. To restrict the number of representative environmental conditions investigated, the k-means clustering method has been applied to select 10 representative sea states and their most probable mean wind speed values at the hub height. Note that the probability of occurrence of each environmental condition has been recalculated to maintain the total wave power flux at the deployment site. It is important to mention that from the design perspective, the hybrid system will have to conform to IEC 61400-3-2 (FOWT) [63] and IEC 62600-2 (WEC) [64] standards.

2.3.1. New south Wales/Sydney

In Sydney, the prevailing wave direction predominantly originates from the southeast. This phenomenon can be attributed to the prevalent wind patterns and oceanographic circumstances that prevail in the given area. However, it is important to note that the state of the waves can experience fluctuations over the course of the year, which can result in the occurrence of waves originating from other directions, such as northeast or east, particularly during specific seasons or weather-related occurrences. The mean annual wind velocity at Sydney's coastal location is approximately 18–28 kilometres per hour. The detailed observations for the Sydney Sea site can be seen in Table 2.

2.3.2. Victoria/Gippsland

In the Gippsland region of Victoria, Australia, the prevalent direction of waves is typically from the southern to southwestern sectors. This occurrence can be attributed to the predominant wind patterns as well as the influence of oceanic currents within the vicinity. Nevertheless, it is noteworthy that the wave direction in Gippsland is susceptible to variation contingent upon local circumstances, coastal features, and atmospheric conditions. Table 3 describe the technical details of wave and wind information at the Gippsland Sea site. During specific meteorological incidents or seasonal fluctuations, waves originating from alternative compass directions, such as southeast or east, may also manifest. It is essential to acknowledge that the wave direction can undergo alterations over the year and even within shorter temporal intervals.

2.3.3. South Australia/Port Lincoln

In the region of Port Lincoln in South Australia, the prevailing direction of waves is typically from the southwest to the south. This occurrence is influenced by the prevailing winds and oceanographic conditions in the vicinity. The Southern Ocean, situated to the south of Port Lincoln, generates waves that propagate towards the coastline, leading to a predominant wave direction from the southwest to the south. Table 4 shows the characteristics of wave and wind at the Port Lincoln site. However, it is noted that the direction of waves can vary based on local weather patterns, seasonal modifications, and coastal characteristics. During specific weather events or under particular circumstances, waves from other directions, such as the west or southeast, may also be observed in Port Lincoln.

2.3.4. Western Australia/Cliff Head

In the Cliff Head region of Western Australia, the dominant wave orientation typically originates from the west to the southwest. This phenomenon is influenced by the prevailing atmospheric winds and oceanic conditions within the vicinity. Due to its exposure to the Indian Ocean, the area experiences the propagation of waves generated by westerly and southwesterly winds, consequently leading to a prevalent wave direction from the west to the southwest. Table 5 represents the details of Cliff Head's wave and wind.

2.4. Performance measures

The performance of the hybrid wave-wind system is analysed using two criteria: average annual power production of three WECs, and the effect of the WECs on the floating platform and wind turbine expressed in terms of the wind turbine nacelle acceleration.

The average power generated by three WECs in one environmental condition defined by (H_s, T_p, U_w) is evaluated as [65]:

$$\bar{P}^{WEC} = B_{pto} \sum_i \sigma^2_{\dot{q}^{wec,i}_{rel}},\qquad(24)$$

where B_{pto} is the WEC PTO damping coefficient, and $\sigma_{\dot{q}^{WEC,i}_3}$ denotes the standard deviation of the relative velocity between the ith WEC and the platform. The annual average power production of three WECs for a particular deployment site with a known probability of occurrence $O(H_s, T_p, U_w)$ of each environmental condition is estimated as:

$$\bar{P}^{WEC}_{site} = \sum_{10} O(H_s, T_p, U_w) \cdot \bar{P}^{WEC}(H_s, T_p, U_w).\qquad(25)$$

The wind turbine performance is characterised by the horizontal component of the wind turbine nacelle acceleration [66]:

$$\ddot{q}^{nac}_1 = \ddot{q}^{fowt}_1 + \ddot{q}^{fowt}_5 L_t.\qquad(26)$$

As nacelle acceleration fluctuates around zero, it is more representative to calculate its standard deviation $\sigma_{\ddot{q}^{nac}_1}$ for each environmental condition of interest. Then, the annual average standard deviation of the nacelle acceleration is calculated as:

$$\bar{\sigma}_{\ddot{q}^{nac}_{1,site}} = \sum_{10} O(H_s, T_p, U_w) \cdot \bar{\sigma}_{\ddot{q}^{nac}_1}(H_s, T_p, U_w).\qquad(27)$$

Key performance measures of the hybrid wind-wave system specified in Eqs. (25) and (27) are penalised (refer to Section 3.2) when the WEC motion exceeds the physical limits of the platform dimensions. Due to the fact that each WEC travels along the platform's side column, the column's height (L^{fowt}_{sc}) can be used as a constraint to prevent unrealistic motion of WECs. Therefore, the constraint is formulated as:

$$L^{fowt}_{sc} - H^{wec} - 3\sigma_{q^{wec,i}_{rel}} > 0,\qquad(28)$$

where L^{fowt}_{sc} is the height of the CSC semi-submersible platform's side column, H^{wec} is the WEC draught, and $3\sigma_{q^{wec,i}_{rel}}$ corresponds to 99.7% of the WEC relative displacement in a particular sea state.
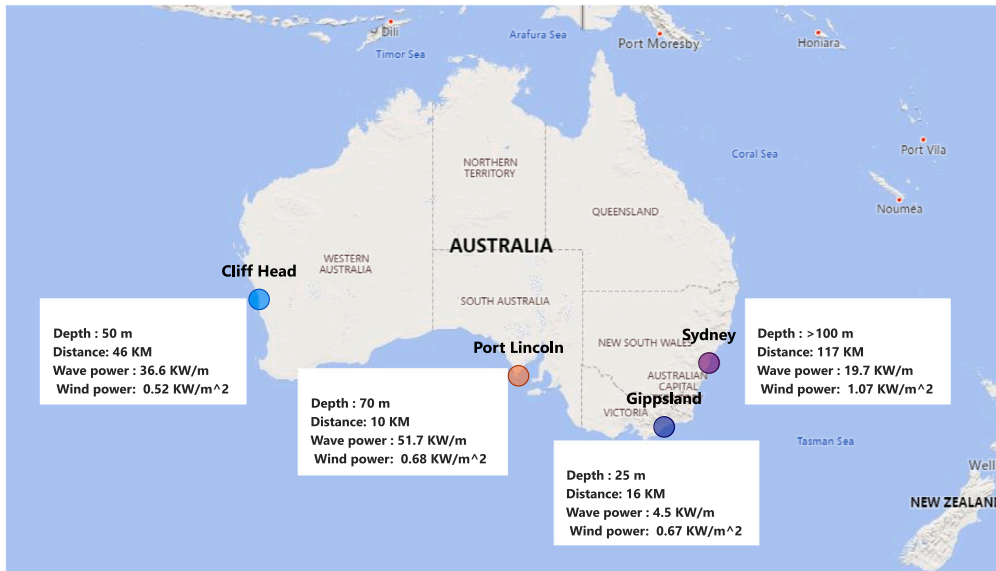
Fig. 4. Geographical location and characteristics of four sea sites, Sydney, Gippsland, Port Lincoln, and Cliff Head.

Table 2
Characteristics and details of Sydney Sea site.

Location	34.0° S 152.3° E
Distance to shore	117 km
Water depth	> 100 m
Mean wave power	19.7 kW/m
Mean wind power	1.07 kW/m²

Table 3
Characteristics and details of Gippsland Sea site.

Location	38.9° S 146.9° E
Distance to shore	16 km
Water depth	25 m
Mean wave power	4.5 kW/m
Mean wind power	0.67 kW/m²

Table 4
Characteristics and details of Port Lincoln Sea site.

Location	34.9° S 135.5° E
Distance to shore	10 km
Water depth	70 m
Mean wave power	51.7 kW/m
Mean wind power	0.68 kW/m²

Table 5
Characteristics and details of Cliff Head Sea site.

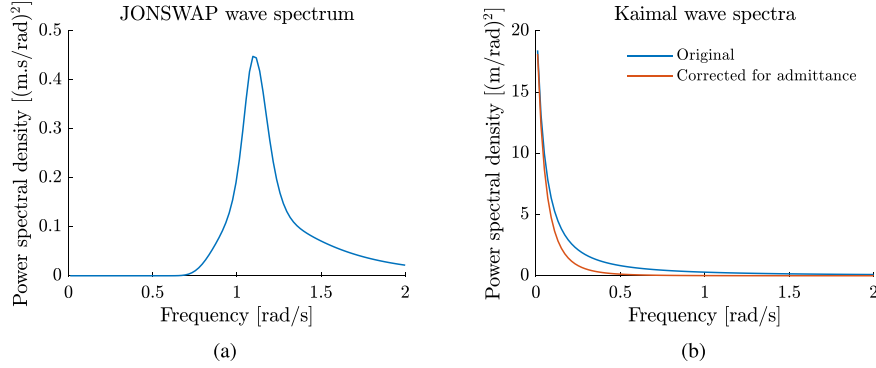| Location	29.5° S 114.8° E
Distance to shore	46 km
Water depth	50 m
Mean wave power	36.6 kW/m
Mean wind power	0.52 kW/m^2

Fig. 5. (a) JONSWAP wave spectrum for $H_s = 1.6$ s, $T_p = 5.7$ m, and $\gamma = 3.3$; (b) Kaimal wind spectrum [67] with the turbulence length scale of 170 m and turbulence intensity of 0.12 for offshore locations.

2.5. Workflow

This section demonstrates the step-by-step procedure to evaluate the power production of WECs and the wind turbine nacelle acceleration for a given environmental condition H_s, T_p and U_w for WECs that have an external radius of $r^{WEC} = 5$ m, a draught of $H^{WEC} = 5$ m, and PTO parameters are set to $K_{pto} = 10^5$ N/m and $B_{pto} = 10^5$ N s/m.

Step 1. Calculate the hydrodynamic parameters of a four-body system consisting of the floating platform and three WECs: $\mathbf{A}_{rad}(\omega)$, $\mathbf{B}_{rad}(\omega)$, $\mathbf{K}_{hs}$, and $\hat{\mathbf{f}}_{exc}(\omega)$.

Step 2. Evaluate the mooring stiffness matrix for a range of platform's positions in surge, heave and pitch $\mathbf{K}_{moor}(\mathbf{q}^{fout})$.

Step 3. Obtain the power and thrust coefficients of a 5-MW reference wind turbine $C_p(\lambda, \beta)$ and $C_T(\lambda, \beta)$.

Step 4. Set environmental conditions H_s, T_p and U_w. In this test case, the first condition from the Sydney site is used: $H_s = 1.6$ m, $T_p = 5.7$ m and $U_w = 13$ m/s.

Step 5. Evaluate the wave $(H_s, T_p) \rightarrow S_\eta(\omega)$ and wind $U_w \rightarrow S_u(\omega)$ spectra, as shown in Fig. 5.

Step 6. Calculate the power spectral density (PSD) of the wave and wind excitation using S_η and $\hat{\mathbf{f}}_{exc}$:

$$\mathbf{S}_{\mathbf{F}}(\omega) = S_\eta(\omega)\hat{f}_{exc}(\omega)\hat{f}_{exc}^*(\omega) + S_u(\omega)\chi^2(\omega)\mathbf{T}\mathbf{T}^*, \tag{29}$$

where ()* denotes the conjugate transpose of a vector/matrix.

Step 7. Evaluate the hybrid system transfer function from Eq. (21):

$$\mathbf{H}(\omega) = \left[-\omega^2(\mathbf{M} + \mathbf{A}_{rad}) + i\omega(\mathbf{B}_{rad} + \mathbf{B}_{eq} + \mathbf{B}_{pto} + \mathbf{B}_{WT})\right.$$
$$\left. + \mathbf{K}_{hs} + \mathbf{K}_{moor} + \mathbf{K}_{pto}\right]^{-1}, \tag{30}$$

where $\mathbf{B}_{eq} = \mathbf{0}_{9\times9}$ in the first iteration.

Step 8. Calculate the PSD matrix of the system state vector $\mathbf{q}$:

$$\mathbf{S}_{\mathbf{q}}(\omega) = \mathbf{H}(\omega)\mathbf{S}_{\mathbf{F}}(\omega)\mathbf{H}^*(\omega). \tag{31}$$

Step 9. Compute the covariance matrix of the displacement and velocity:

$$\sigma_{\mathbf{q}}^2 = \text{cov}[\mathbf{q}, \mathbf{q}] = \int_0^\infty \mathbf{S}_{\mathbf{q}}(\omega)d\omega, \tag{32}$$

$$\sigma_{\dot{\mathbf{q}}}^2 = \text{cov}[\dot{\mathbf{q}}, \dot{\mathbf{q}}] = \int_0^\infty \omega^2 \mathbf{S}_{\dot{\mathbf{q}}}(\omega)d\omega. \tag{33}$$

Step 10. Estimate the equivalent viscous damping matrix $\mathbf{B}_{eq}$ following the procedure explained in [65].

Step 11. Evaluate the PSD of the relative WEC displacement $q_{rel}^{wec,i}$ and of the wind turbine nacelle acceleration $\ddot{q}_1^{nac}$ using $\mathbf{S}_{\mathbf{q}}(\omega)$ and Eqs. (2) and (26), respectively. For the case considered in this section, the power spectral densities of the relative WEC displacement and velocity are shown in Fig. 6. The corresponding values of the relative WEC velocities are evaluated using Eq. (33) and equal to $\sigma_{\dot{q}_{rel}^{wec,1}}^2 = 0.0419$, $\sigma_{\dot{q}_{rel}^{wec,2}}^2 = \sigma_{\dot{q}_{rel}^{wec,3}}^2 = 0.0526$, and the WEC power in this case would be 14.7 kW that is obtained using Eq. (24). The standard deviation of the horizontal component of the wind turbine nacelle acceleration is $\sigma_{\ddot{q}_1^{nac}} = 0.1316$.

3. Optimisation setup

Two optimisation functions are introduced in this paper: maximisation of WEC annual power production $\bar{P}_{site}^{WEC}$, and minimisation of the wind turbine nacelle acceleration $\bar{\sigma}_{\ddot{q}_{1,site}^{nac}}$ subject to the WEC design (radius r^{WEC} and draught H^{WEC}) and control parameters (PTO stiffness K_{pto} and damping B_{pto}). The design variables and their limits are demonstrated in Table 6.

Minimise: $F(\vec{x}) = [f_1(\vec{x}), f_2(\vec{x})]$,

$$\begin{cases} f_1 = 1/\bar{P}_{site}^{WEC} & \vec{x} = [r^{WEC}, H^{WEC}, K_{pto}^1, \dots, K_{pto}^m, B_{pto}^1, \dots, B_{pto}^m] \\ f_2 = \bar{\sigma}_{\ddot{q}_{1,site}^{nac}}, \end{cases}$$
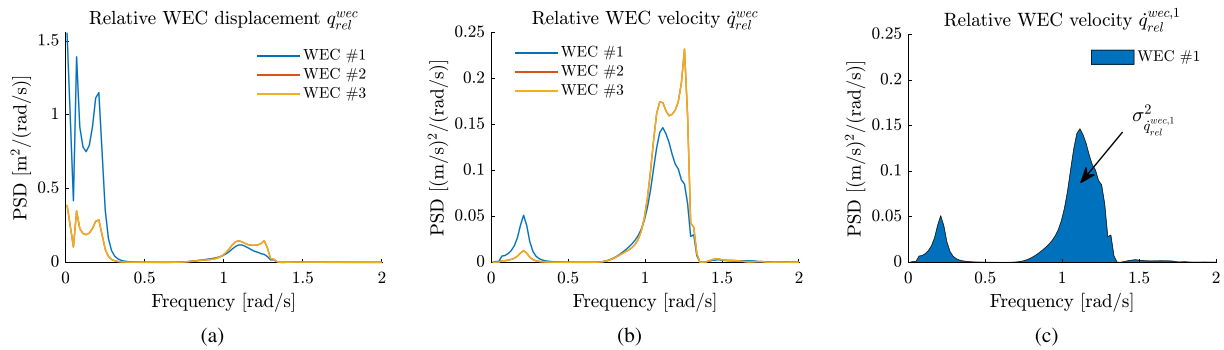
$$\tag{34}$$

Fig. 6. (a) PSD of the WEC relative displacement; (b) PSD of the WEC relative velocity; and (c) demonstration of how the standard deviation is calculated using the PSD values.

Table 6
Design variables.

Parameter	Unit	Values
WEC outer radius (r^{WEC})	m	[5, 6, 7, 8, 9, 10]
WEC draught (H^{WEC})	m	[6, 7, 8, 9, 10, 11, 12, 13, 14, 15]
PTO stiffness (K_{pto})	N/m	$[0\dots 10^{10}]$
PTO damping (B_{pto})	N/(m/s)	$[0\dots 10^{10}]$

Subject to :
$$g_i(\vec{x}) \geq 0, \ i = 1, 2, \dots, M_n \tag{35}$$

$$h_i(\vec{x}) = 0, \ i = 1, 2, \dots, P_n \tag{36}$$

$$L_i \leq x_i \leq U_i, i = 1, 2, \dots, N \tag{37}$$

where N denotes the count of variables under consideration. Meanwhile, g_i and M_n stand for the number and ith inequality constraints and h_i and P_n represent the count and ith equality constraints. Lastly, $[L_i, U_i]$ refers to the boundaries of the ith variable.

3.1. Pareto dominance

Pareto Dominance, a fundamental concept in the field of multiobjective optimisation, elucidates the intricate relationship among diverse solutions in the objective space. By employing Pareto dominance as a pivotal criterion, multiobjective optimisation techniques can furnish an assortment of solutions that embody the most advantageous compromises between conflicting objectives. This enables decision-makers to make judicious selections grounded upon their individual preferences and priorities [68].

Suppose that there are two vectors such as: $\vec{S1} = (S1_1, S1_2, \dots, S1_k)$ and $\vec{S2} = (S2_1, S2_2, \dots, S2_k)$. Vector $S1$ dominates vector $S2$ (denote as $S1 \succ S2$) iff :

$$\forall i \in \{1, 2, \dots, k\}, \left[f\left(S1_i\right) \geq f\left(S2_i\right) \right] \wedge \left[\exists i \in 1, 2, \dots, k : f\left(S1_i\right) \right] \tag{38}$$

A solution $\vec{S1} \in X$ is called Pareto-optimal iff:

$$\nexists \vec{S2} \in X \mid F(\vec{S2}) \succ F(\vec{S1}) \tag{39}$$

The set of all Pareto-optimal solutions is called the Pareto set as follows:

$$P_S := \{S1, S2 \in X \mid \exists F(S2) \succ F(S1)\} \tag{40}$$

Finally, the Pareto optimal front is a set including the objective functions value for the Pareto solutions set:

$$P_f := \left\{ F(S1) \mid S1 \in P_s \right\} \tag{41}$$

3.2. Constraint handling

The prevalent technique within the optimisation community to tackle limitations, especially when it comes to disparities, involves the utilisation of penalties [69]. The concept behind the penalty function

is to convert a problem of constrained optimisation into one that is unconstrained by incorporating a specific value to the objective function based on the extent of violation of the constraints found within a particular solution. The most commonly employed approach in optimisation methods is the exterior penalty method. In this way, we may commence with an infeasible solution and gradually progress towards the feasible region. This function does not necessitate an initial feasible solution. The general structure of the exterior penalty function [69] is as follows:

$$\phi(\vec{x}) = f(\vec{x}) \pm \left[\sum_{i=1}^{n} r_i \times G_i + \sum_{j=1}^{p} c_j \times H_j \right] \tag{42}$$

where $\phi(\vec{x})$ is the modified objective function that should be optimised, G_i and H_j are components of inequality and equality constraints $g_i(\vec{x})$ and $h_j(\vec{x})$, respectively, and r_i and c_j are penalty factors.

For the hybrid wind-wave system design, the constraint is governed by the allowable displacement of WECs (refer to Eq. (28)). Introducing a variable that corresponds to the allowable displacement of the wave energy system in one environmental condition n:

$$\Delta_n = L_{sc}^{FOWT} - H^{WEC} - \max_i \left(3\sigma_{q_3^{WEC,i}}\right), \quad i = 1, 2, 3. \tag{43}$$

The modified performance measures that take into account WEC motion constraints are formulated as follows:

$$\hat{P}^{WEC} = \begin{cases} \max\left(1, \bar{P}_{site}^{WEC} - \left(\mid \sum_n^N \Delta_n \mid \times P_{f1}\right)\right) + \epsilon, & \text{if } \Delta_n < 0, \\ \bar{P}_{site}^{WEC}, & \text{otherwise.} \end{cases} \tag{44}$$

$$\hat{\sigma}_{\ddot{q}_1^{nac}} = \begin{cases} \bar{\sigma}_{\ddot{q}_{1,site}^{nac}} + \left(\mid \sum_n^N \Delta_n \mid / P_{f2}\right) & \text{if } \Delta_n < 0, \\ \bar{\sigma}_{\ddot{q}_{1,site}^{nac}} & \text{otherwise.} \end{cases} \tag{45}$$

The values of penalty factors are set to $P_{f1} = 100$ and $P_{f2} = 10$.

4. Methods

4.1. Multi-objective optimisation algorithms

Multi-objective optimisation algorithms (MOOA) are optimisation algorithms developed to figure out problems with multiple objectives. These algorithms are designed to discover an optimal candidate for a problem by satisfying multiple objectives simultaneously [70,71]. By taking into account multiple objectives in the decision-making process, MOOA is able to propose a more comprehensive and accurate landscape of the problem than a single-objective algorithm [72,73].

MOOA can be categorised into two primary groups: evolutionary algorithms and multi-objective search algorithms. Evolutionary algorithms involve using a population of solutions that evolve over time to reach an optimal solution. Examples of evolutionary algorithms include search algorithms based on genetic operators, simulated annealing, and

Table 7

The configuration details of multi-objective optimisation methods employed in the hybrid wave-wind converter problem.

	Abbreviation	Full name	Initial settings
1	NSGA-II [24]	Non-dominated Sorting Genetic Algorithm	$P_{Cros} = 0.7$, $N_{Cros} = 2 \times round(P_{Cros} \times N_{pop}/2)$, $P_{Muta} = 0.4$, $N_{Muta} = round(P_{Muta} \times N_{pop})$, $\rho = 0.02$, $\sigma = 0.1 \times (Max_{var} - Min_{var})$.
2	MOEA/D [48]	Multi-Objective Evolutionary Algorithm based on Decomposition	$N_{Archive} = N_{pop}$, $N_{nei} = max((0.15 \times N_{pop}), 2)$, $\gamma = 0.5$, $\alpha = urand(-\gamma, 1 + \gamma)$,
3	PESA-II [44]	Pareto Envelope-based Selection Algorithm	$N_{Archive} = N_{pop}$, $N_{Grid} = 7$, $Inflation_f = 0.1$, $\beta_{del} = 1$, $\beta_{sel} = 2$, $P_{Cross} = 0.5$ $N_{Cross} = 2 \times round(P_{Cross} \times N_{pop}/2)$, $P_{Muta} = 1 - P_{Cross}$, $N_{Muta} = N_{pop} - N_{Cross}$, $\gamma = 0.15$, $h = 0.3$
4	MOPSO [49]	Multi-Objective Particle Swarm optimisation	$N_{Rep} = 20$, $Inertia_{Weight} = 0.5$, $Damp_{rate} = 0.99$, $C_I = 1$, $C_{II} = 2$, $N_{grid} = 7$, $\alpha = 0.1$, $\beta = 2$, $\gamma = 2$, $Mutation_{Rate} = 0.1$
5	MOGWO [31]	Multiple Objective Grey Wolf optimiser	$N_{Archive} = N_{pop}$, $\alpha_g = 0.1$, $N_{Grid} = 10$, $\beta_g = 4$, $\gamma_g = 2$
6	MALO [46]	Multi-objective Ant Lion optimiser	$N_{Archive} = N_{pop}$, $r = (Max_{var} - Min_{var})/2$, $V_{max} = (Max_{var} - Min_{var})/10$
7	MODA [47]	Multi-Objective Dragonfly Algorithm	$N_{Archive} = N_{pop}$, $r = \frac{(Max_{var} - Min_{var})}{4} + ((Max_{var} - Min_{var}) \times (\frac{iter}{max_{iter}}) \times 2)$, $w = 0.9 - iter \times ((0.9 - 0.2)/max_{iter})$, $C = 0.1 - iter \times ((0.1 - 0)/(\frac{max_{iter}}{2}))$
8	SPEA-II [45]	Strength Pareto Evolutionary Algorithm II	$N_{Archive} = N_{pop}$, $P_{Cross} = 0.7$, $N_{Cross} = 2 \times round(P_{Cross} \times N_{pop}/2)$, $P_{Muta} = 0.3$, $N_{Muta} = round(P_{Muta} \times N_{pop})$, $\gamma = 0.1$, $h = 0.2$

PSO [74]. Multi-objective search algorithms [75] involves the use of a search space with regard to exploring an optimal solution.

In addition to these two main categories, there are also hybrid algorithms that combine elements of both evolutionary algorithms and multi-objective search algorithms [76]. These hybrid algorithms are often used to improve the search process's efficiency and accuracy. MOOA are commonly used in a variety of fields, including renewable energy systems [77], engineering, economics, finance, and operations research. These algorithms are also useful in medical, aerospace, and military applications. By taking into account multiple objectives, MOOA can provide a more accurate picture of the problem and lead to better decision-making. The technical settings of the multi-objective optimisation methods applied in this study can be seen in Table 7. N_{pop} is the initial population size at 50. ρ and σ are mutation rate and mutation step size, respectively, N_{nei} is the number of neighbours, α_g is the grid inflation parameter, β_g is the leader selection pressure parameter, γ_g is the extra (to be deleted) repository member selection pressure rate.

4.1.1. Non-dominated Sorting Genetic Algorithm II (NSGA-II)

NSGA-II (Non-dominated Sorting Genetic Algorithm II) [24] is a population-based multi-objective evolutionary algorithm (MOEA) introduced by K. Deb et al. in 2002. NSGA-II is an enhanced version of the original NSGA algorithm developed by Srinivas and Deb in 1995 [78]. NSGA-II is a popular MOEA that is applied to figure out optimisation problems with multiple conflicting objectives. It is an extension of the Pareto-optimal concept, which suggests that a decision is optimal if no other decision is better in all objectives.

The fundamental insight behind NSGA-II is to find a set of Pareto-optimal solutions which cannot be enhanced in one objective without destructing the others. The approach begins by selecting a population of random individuals, each with a set of parameters. It then evaluates the individuals and sorts them into a non-dominated front based on the objectives. The algorithm then uses a combination of various mutation and crossover operators to make the next generation of offspring from the non-dominated front. Finally, it selects new individuals and replaces the old ones in the population. NSGA-II has been widely used [79] in a wide range of fields, such as engineering design, water resources management, renewable energy [80], power systems [81] and economics. It is also used in the design of neural networks, intelligent systems, and robotic control systems.

4.1.2. Multiple objective grey wolf optimiser (MOGWA)

One of the most popular swarm-based intelligence methods is MOGWA [31]. Indeed, MOGWA is an extended model of GWO with a single objective and is used to figure out MOO problems. It is inspired by the behaviour of grey wolves in nature, where they interact with each other to search for their prey. The algorithm works on a population of solutions, called individuals, and evolves them towards optimal solutions by using a set of operators. These operators include selection, mutation and crossover. MOGWA is based on the idea of the dominance of the fittest and makes use of the grey wolf pack behaviour to enhance its performance and show successful performance in power systems [82] compared with other MOO methods. MOGWA was initially proposed by Mirjalili et al. [31] in their paper "Grey Wolf Optimiser" in 2016. Since then, this algorithm has been developed to solve various optimisation problems such as engineering design optimisation, medical image segmentation, and clustering. Compared to other multi-objective optimisation algorithms, MOGWA has demonstrated better performance and stability [83].

4.2. Proposed new adaptive chaotic multi-objective grey wolf optimisation method

Recent comprehensive studies manifest that the GWO application to resolve MOO problems has seen swift growth. All these algorithms share the same characteristic of using a predetermined-size archive external to the optimisation process to record the Pareto optimal solutions and then updating the archive through various archiving strategies and density metrics [84]. Nevertheless, very few MOGWAs consider the importance of search strategies on the pool based on the input from the dominant solutions that are recorded in the collection, which is a significant operation that impacts the algorithm's convergence. Additionally, most real engineering multi-objective problems have several boundary restrictions that limit the search area; if a potential algorithm solution moves beyond the search objective, then a course of action should be taken to handle the breach of the boundary restrictions.

This paper looks to bridge the shortage between theoretical research and practical multi-objective applications by introducing an enhanced and chaotic version of the MOGWA algorithm with various search strategies, referred to as DMOGWA. The DMOGWA's key advantages include an adaptive chaotic control search strategy and neighbourhood search with a dynamic archive size based on the diversity of the

population. The technical details of the DMOGWA's components are as follows.

4.2.1. Encircling step

Previously [31], it was mentioned that grey wolves form a social hierarchy and encircle their quarry when hunting. This encircling action can be simulated mathematically as follows.

$$\vec{E} = |\vec{D}.\vec{Z}_p(t) - \vec{Z}(t)| \tag{46}$$

$$\vec{Z}(t+1) = \vec{Z}_p(t) - \vec{B}.\vec{E} \tag{47}$$

where $\vec{E}$ represents the length between the prey coordination $\vec{X}_p$ with another associate $\vec{Z}$ in the general iteration(t). Likewise, the vectors $\vec{B}$ and $\vec{D}$ recreate an essential function, holding a significant effect for tuning the exploration and exploitation demeanours and are summed by Eqs. (48) and (50):

$$\vec{B} = 2.\vec{\beta}.\vec{rand}_1 - \vec{\beta} \rightarrow 0 \leq a \leq 2 \tag{48}$$

$$\beta = 2 - iteration.(\frac{2}{Max_{iteration}}) \tag{49}$$

$$\vec{D} = 2.\vec{rand}_2 \tag{50}$$

where β has been linearly decreased between 2 to 0 through the runtime. $rand_1$ and $rand_2$ are random vectors between 0 and 1.

4.2.2. Hunting step

The capacity of grey wolves to recognise the whereabouts of their prey and form a ring around them is remarkable, with the alpha wolf usually taking the lead. Beta and delta wolves occasionally take part in the hunt, but since the location of the prey is typically unknown in an obscure area, simulating the hunting behaviour of these wolves mathematically requires that the wolves with the foremost three solutions are assumed to be the alpha, beta and delta wolves, respectively. The remaining candidates are then considered omega wolves and must revise their coordination based on the alpha, beta and delta wolves. In this regard, the novel location of the grey wolves can be determined, as described by the following formulas (Eqs. (51)–(53)).

$$\vec{Z}(t+1) = \frac{\vec{Z}_1 + \vec{Z}_2 + \vec{Z}_3}{3} \tag{51}$$

$$\vec{Z}_1 = \vec{Z}_\alpha(t) - \vec{B}_1.\vec{E}_\alpha, \vec{Z}_2 = \vec{Z}_\beta(t) - \vec{B}_2.\vec{E}_\beta$$
$$\vec{Z}_3 = \vec{Z}_\delta(t) - \vec{B}_3.\vec{E}_\delta \tag{52}$$

$$\vec{E}_\alpha = |\vec{B}_1.\vec{Z}_\alpha - \vec{Z}|, \vec{E}_\beta = |\vec{B}_2.\vec{Z}_\beta - \vec{Z}|$$
$$\vec{E}_\delta = |\vec{D}_3.\vec{Z}_\delta - \vec{Z}| \tag{53}$$

4.2.3. Adaptive chaotic control search step

Previous research has suggested various strategies for modifying the hyper-parameters of GWO, but they still need to take into account the performance of the GWO during runtime. This paper proposes a flexible strategy for altering the control variable of multi-objective GWO. This allows the optimisation procedure to be monitored. After a pre-defined number of replications where the idea candidate in each generation does not exceed the alpha particle, the control parameter should be adjusted again. Furthermore, a chaotic sequence is embedded by mapping it through a normalising function to provide good stability between exploitation and exploration. The significant contributions of this proposed method are:

- To attain the highest outcome, a chaotic series is generated and blended with the control variable (β) for each cycle. The most effective chaotic map is employed to accomplish this [85]. Eq. (51)

stipulates the chaotic map (Piecewise) utilised in the adaptive method.

$$z_{i+1} = \begin{cases} \frac{z_i}{\xi} & 0 \leq z_i < \xi \\ \frac{z_i - \xi}{0.5 - \xi} & \xi \leq z_i < 0.5 \\ \frac{1 - \xi - z_i}{0.5 - \xi} & 0.5 \leq z_i < 1 - \xi \\ \frac{1 - z_i}{\xi} & 1 - \xi \leq z_i < 1 \end{cases}, \xi = 0.4 \tag{54}$$

- The normalisation function should be applied periodically to even out the erratic pattern of the sequence, with the mathematical model of the function depicted in Eq. (55).

$$N_i = \theta_i^{Max} - (\frac{\theta_i^{Max} - \theta_i^{Min}}{Max_{it}}) \times it \tag{55}$$

where $\theta_i^{Max} = 0.2$ and $\theta_i^{Min} = 10^{-4}$ are the highest and lowest possible values for the normalisation function. θ_i^{Max} and θ_i^{Min} can manage the randomness of the utilised chaotic map and alternate between the exploration and exploitation steps cyclically. The greatest amount of iterations in each cycle is denoted as Max_{it}, leading to the calculation of the normalised chaotic values (η_{it}) via Eq. (56).

$$\eta_{it} = N_i * \epsilon \tag{56}$$

where the proposed chaotic map produces the ϵ. The chaotic sequence is combined with the control vector $\vec{\beta}$ and is defined using Eq. (57).

$$\beta = (2 - \theta_i^{Max}) - (it^2 \times \frac{2 - \theta_i^{Max}}{Max_{it}^2}) + \eta_{it} \tag{57}$$

A novel approach named CMOGWA (Combination of adaptive chaotic control search steps with MOGWA) has been proposed as an initial effort to enhance the performance of MOGWA in terms of exploitation and robustness. By incorporating a chaotic sequence in the control search step, CMOGWA aims to improve MOGWA's exploration capability by enabling more effective exploration of the search space and the discovery of diverse solutions. This integration of chaos helps mitigate the issue of premature convergence and facilitates the identification of a wide range of Pareto optimal solutions in multiobjective optimisation problems. The embedding of a chaotic sequence within the control search step offers the potential for significant improvements in the performance and effectiveness of the MOGWA algorithm, ultimately leading to enhanced optimisation outcomes in complex and challenging optimisation scenarios.

4.2.4. Adaptive archive size based on diversity

In standard MOGWA algorithms, the archive with a fixed size serves as a pool for non-dominated candidates discovered throughout the optimisation process, characterising the Pareto front—a representation of the trade-offs between conflicting objectives [86]. The various situations for updating the archive (See Fig. 7) are as follows.

- The nondominated vectors discovered during each iteration in the primary population undergo a comparison process with the contents of the repository, which is initially empty. This comparison is performed on a one-to-one basis. If the external archive is found to be empty, the current solution is accepted.
- However, if the new solution is dominated by any individual within the external archive, it is automatically discarded.
- On the other hand, if none of the elements in the external population dominates the solution attempting to enter, it is stored in the external archive.
- In the event that the archive contains solutions that are dominated by the new element, those solutions are removed from the archive
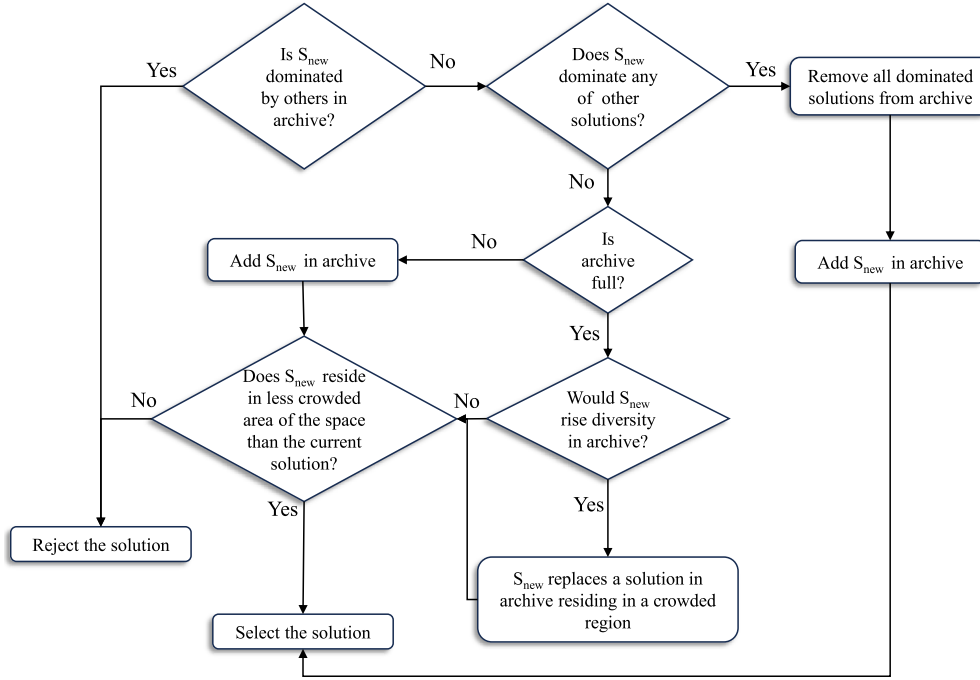
Fig. 7. The flowchart of updating MOGWO's archive.

- Lastly, the adaptive grid procedure is invoked if the external population has reached its maximum capacity. This procedure ensures the external archive does not exceed its allowable limit.

The archive size plays a pivotal role in adjusting the convergence speed of the algorithm. A smaller archive size facilitates faster convergence by focusing on a restricted set of non-dominated solutions. In contrast, a larger archive size prioritises maintaining a more diverse range of solutions, which can result in a slower convergence rate but offers improved coverage of the Pareto front [87]. However, it is essential to note that a larger archive may include redundant or less significant solutions, potentially diluting the quality of the overall representation. On the other hand, a smaller archive size concentrates on a limited set of high-quality solutions. While this focus ensures the preservation of solutions with superior characteristics, it runs the risk of overlooking certain regions of the Pareto front, potentially disregarding valuable trade-off solutions.

To confront these challenges, we propose an adaptive mechanism that adjusts to the changing circumstances and dynamically modifies the size of the archive throughout the steps of optimisation. Our approach harnesses specific measures of diversity, particularly the concept of crowding distance, to govern the adaptive nature of the archive's dimensions. Crowding distance acts as a metric, quantifying the degree to which a solution is enveloped or crowded by neighbouring solutions within the realm of objectives. It effectively estimates the local density of solutions and plays a pivotal role in upholding a multitude of different possibilities within the population. A higher value of crowding distance signifies that a solution resides within a more sparse region of the objective landscape, wherein fewer neighbouring solutions exist in close proximity. In contrast, a lower crowding distance implies that a solution is encircled by nearby solutions, indicating a higher density within that particular region. By harnessing the power of crowding distance as a benchmark, our adaptive mechanism dynamically adjusts the archive's size with every iteration, ensuring that the population preserves a diverse array of solutions and thoroughly explores the entirety of the objective space. In order to compute the sum of the crowding distance for each solution

in the population, Eq. (58) is introduced.

$$Sum_{cd} = \sum_{i=1}^{N_{pop}} (I[i]_{cd} + (I[i+1]m - I[i-1]m)/\left(f_m^{mix} - f_m^{nin}\right)) \tag{58}$$

where $I[i]_{cd}$ is the ith solution's crowding distance in non-dominated pareto based on mth objective in the optimisation. $I[i]m$ is ith solution's mth objective value. f_m^{max} and f_m^{min} are the maximum and the minimum of mth objective value, respectively.

To formulate the adaptive adjustment of the archive size based on the sum of the crowding distance, we define a threshold value, denoted as α. If the sum of the crowding distance is less than this threshold, it indicates that the diversity in the population is insufficient. Therefore, the archive size should be increased as a coefficient (θ) of the non-dominated solution number. Conversely, suppose the sum of the crowding distance exceeds the threshold. In that case, it suggests that the population is already diverse enough, and the archive size should be decreased to maintain a more focused set of solutions. The formulation can be expressed as follows:

$$Ar_{new}$$
$$= \begin{cases} Ar_{size} + (\theta \times N_{non-dominated}) & \text{if } \sum_{i=1}^{N_{pop}} I[i]_{cd} < \alpha, 0 < \theta < 0.5 \\ max(\frac{N_{pop}}{2}, Ar_{size} - (\theta \times N_{non-dominated})) & Otherwise \end{cases} \tag{59}$$

Based on the analysis presented in Fig. 8, it is evident that a small archive size ($0.1 \times N_p$) exhibits rapid initial convergence; however, it subsequently encounters challenges associated with premature convergence, resulting in suboptimal optimisation outcomes. Conversely, a bigger repository size of 20 (40% of the population) demonstrates significantly improved performance compared to the other sizes. Notably, in this investigation, an adaptive archive size started at 20. It emerged as the optimal choice, striking a balance between convergence speed and avoiding premature convergence, thus yielding desirable optimisation results.
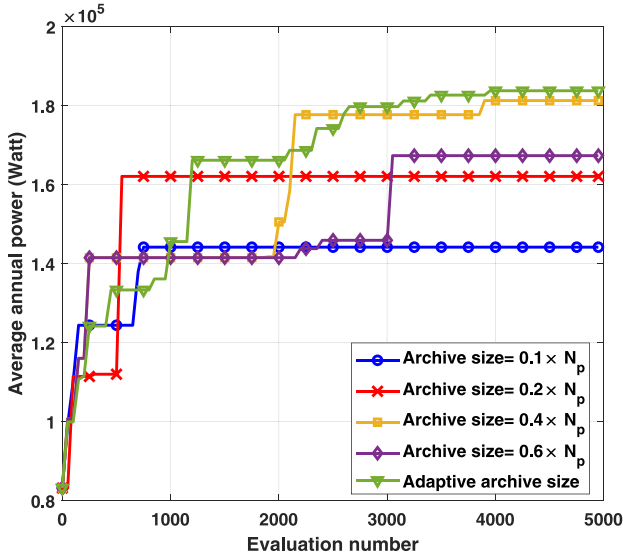
Fig. 8. The effective impact of archive size on the multi-objective optimisation method based on the Sydney sea site.

Fig. 9. Discretisation landscape of PTO parameters search space for Sydney sea site.

4.2.5. Adaptive grid strategy

The MOGWO algorithm [31] incorporates an adaptive grid mechanism to generate Pareto fronts that are evenly distributed. This methodology is derived from a modified version of the adaptive grid proposed in Refs. [88,89]. The external archive is used to store all solutions that are non-dominated in relation to its contents. The objective function space is divided into regions represented by hypercubes. When an individual is added to the external population and falls outside the current boundaries of the grid, it is necessary to recalculate the grid and relocate each individual within it. The adaptive grid offers computational advantages compared to niching, as it has a lower cost, except in cases where the grid needs to be updated with each generation. In such instances, the computational complexity would be equivalent to niching. The adaptive grid serves the purpose of uniformly distributing a significant number of hypercubes throughout the search space. To achieve this objective, problem-specific information, such as the number of grid subdivisions, is necessary. By utilising the adaptive grid mechanism, the MOGWO algorithm ensures that the obtained Pareto fronts are well-distributed, capturing diverse, high-quality solutions from various regions of the objective function space.

4.2.6. Leaders selection

In the standard GWO algorithm, the search procedure is steered by three outstanding solutions referred to as alpha, beta, and delta wolves. These commanding figures play a pivotal role in guiding other search agents towards promising areas within the search space, intending to discover solutions that are in proximity to the global optimum. Nevertheless, when confronted with a multi-objective search space, the task of comparing solutions becomes intricate due to the existence of Pareto optimality principles. In order to tackle this issue [31], a leader selection mechanism is implemented and employs an archive that stores the most superior non-dominated solutions that have been acquired thus far. The leader selection component identifies the least crowded segments of the search space and chooses one of its non-dominated solutions as the alpha, beta, or delta wolves. The selection procedure uses a roulette-wheel method, where each hypercube is assigned a particular probability.
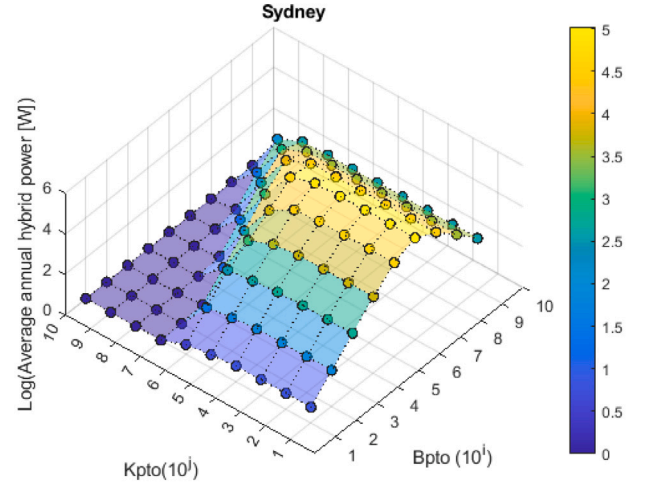
$$P_i = \frac{\zeta}{N p_i} \tag{60}$$

where ζ is a constant value and should be > 1 and $N p$ is the Pareto optimal solutions number achieved in the ith segment.

In Eq. (60), it can be observed that hypercubes exhibiting lower levels of crowding display a higher probability of suggesting novel leaders in the MOGWO algorithm. The likelihood of selecting a hypercube as the source of leaders increases as the number of solutions obtained within that hypercube decreases. However, certain exceptional circumstances arise due to the stipulation of selecting three leaders as follows.

- In this situation, the least crowded segment contains three solutions; all three are randomly designated as alpha, beta, and delta solutions.
- Moreover, in situations where the least crowded hypercube possesses fewer than three solutions, the second least crowded hypercube is also taken into consideration for selecting additional leaders.
- This particular scenario is reiterated if the second least crowded hypercube contains only one solution, whereby the delta leader is chosen from the third least crowded hypercube. This approach guarantees that MOGWO steers clear of selecting similar leaders for alpha, beta, or delta.
- Consequently, the search is consistently directed towards unexplored or unexposed regions of the search space. The leader selection mechanism prioritises the least crowded hypercubes and introduces leaders from different segments if there is an insufficient number of leaders (less than 3) in the least crowded segment.

4.2.7. Discretisation strategy

Given the expansive array of Power Take-Off (PTO) parameters spanning from 10^1 to 10^{10}, compelling exploration across the entire problem domain presents formidable challenges. In order to tackle this predicament, we propose the utilisation of a discretisation technique that facilitates the conversion of continuous PTO parameters into a discretised space employing the logarithm function with a base of 10. This technique effectively diminishes the dimensionality of the search space. It simplifies the optimisation problem by confining the number of feasible solutions and narrowing the focus of the search to specific regions of interest. Fig. 9 illustrates the manner in which the decision variables (PTO parameters) are discretised using the logarithm transfer function.

By implementing the method of discretisation, the optimisation algorithm acquires the capacity to venture into and assess potential
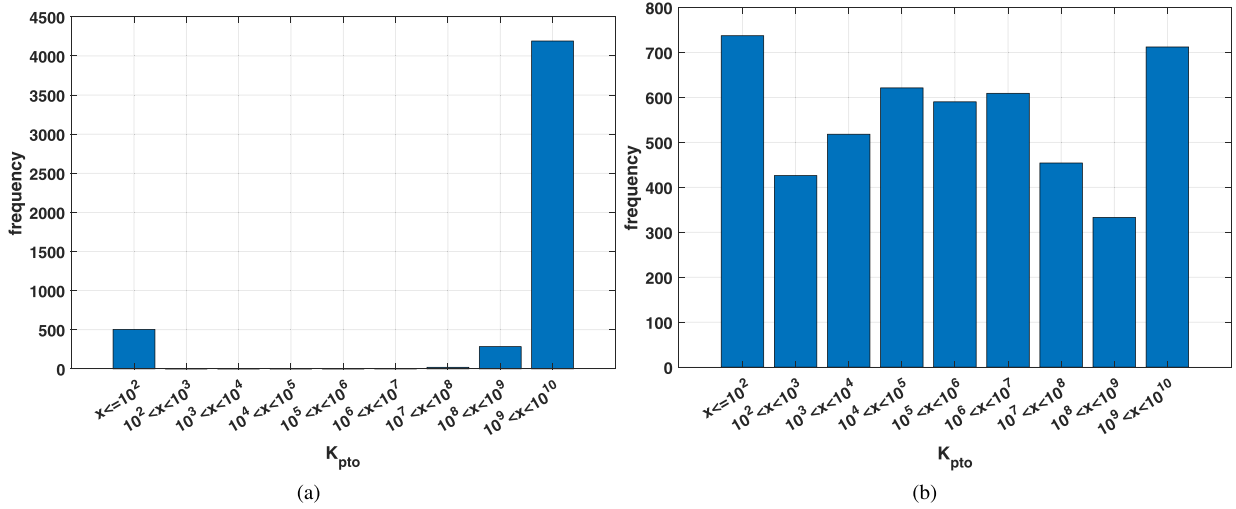
Fig. 10. The distribution of PTO parameter (K_{pto}) for the first population of (a) MOGWA, and (b) DMOGWA with discretisation technique.

solutions in a more efficient manner within the diminished realm of search. The reduced scale permits swifter convergence towards the most optimum solutions by diminishing the burdensome extent of exploration. Furthermore, the computational efficacy of the optimisation process is amplified as the discretised space facilitates more straightforward computations and expedites the evaluation of potential solutions.

As can be seen in Fig. 10(a), there is an imbalanced distribution in the initialisation of the first population using a uniformly random generation between the continuous range of PTO parameters (1.0E+1,1.0E+10). This imbalanced issue can be solved using the proposed discretisation method introduced above, which can be observed in Fig. 10(b). This technique has a constructive impact on the optimisation method to start the search using diverse configurations of the platform.

To have a review of the technical details of the DMOGWA's steps, we list and detail them, which can be seen in Algorithm 1.

5. Numerical results and discussions

5.1. Landscape analysis

Landscape analysis is a technique used in optimisation problems to gain insight into the shape and characteristics of the objective function's landscape. The objective function's landscape refers to the relationship between the input parameters and the function's output values. A landscape analysis of an optimisation problem involves evaluating the objective function over a range of input parameters and examining the resulting output values. This analysis can help identify landscape features that may influence optimisation, such as peaks, valleys, and plateaus [90].

Some standard techniques used in landscape analysis include: (I) Visualisation: Creating 3D plots or heat maps of the objective function's output values as a function of the input parameters can help identify landscape features, such as multiple local optima or narrow ridges. (II) Local search: Applying local search algorithms to sample the objective function's landscape around a given input point can help to identify local optima and estimate the size of the basins of attraction. (III) Random sampling: Randomly sampling the objective function's landscape over a wide range of input parameters can help identify the optimal distribution and the landscape's ruggedness. (IV) Sensitivity analysis: Evaluating the sensitivity of the objective function's output values to small changes in the input parameters can help to identify regions of the landscape that are particularly sensitive to perturbations.

Algorithm 1 Adaptive Chaotic Multi-objective Grey Wolf Optimisation Method

1: **procedure** DMOGWA
2: **Initialise** parameters $a, A, C, \theta_i^{Max}, \theta_i^{Min}, \rho$ and Max_{iter_N}
3: $archive = []$, $Np = 50$ ▷ Initialise archive, Population size
4: $\mathbb{S}$ $=$ $\{\langle r_1, H_1, B_{k_1}^1, ..., B_{k_{10}}^1, B_{d_1}^1, ..., B_{d_{10}}^1 \rangle, ...$
 , $\langle r_{Np}, H_{Np}, B_{k_1}^{Np}, ..., B_{k_{10}}^{Np}, B_{d_1}^{Np}, ..., B_{d_{10}}^{Np} \rangle\}$ ▷ Initial Population
5: $< \hat{P}^{WEC}, \hat{\sigma}_{\bar{q}_1^{nac}} >= Eval([S_1, S_2, ..., S_{Np}])$ ▷ Evaluate Layouts
6: $archive = Non\text{-}dominated(\mathbb{S})$ ▷ Find the non-dominated solutions and update archive
7: X_α=The best layout from $\langle archive \rangle$ ▷ Find three best layouts
8: X_β=The second best layout from $\langle archive \notin X_\alpha \rangle$
9: X_δ=The third best layout from $\langle archive \notin X_\alpha, X_\beta \rangle$
10: **while** *stillTime()* **do**
11:   **for** i in $[1, .., Np]$ **do**
12:    *Update* S_i *by Equation* (51)
13:    **if** S_i *is not feasible* **then**
14:     $f(S_i) = f(S_i) + Penalty(S_i)$ ▷ *Compute violation and apply penalty*
15:    **end if**
16:   **end for**
17:   $< \hat{P}^{WEC}, \hat{\sigma}_{\bar{q}_1^{nac}} >= Eval([S_1, S_2, ..., S_{Np}])$ ▷ *Evaluate Layouts*
18:   $N_{ds} = Non\text{-}dominated(\mathbb{S})$ ▷ *Find Non-dominated solutions*
19:   $archive = Update(archive \cup N_{ds})$
20:   *Update* $archive_{size}$ *by Equation* (59)
21:   **if** $archive_{size} > Max_{size}$ **then**   ▷ *if archive is full*
22:    $archive =$ *Grid Mechanism(archive)* ▷ *Remove worst solution from archive*
23:    $archive =$ *Add(S_{new})*
24:   **end if**
25:   *Update* N_i *and* η_{iter} *by Equation* (55),(56)
26:   *Update* a, A *and* β *by Equation* (57),(50),(49)
27:   **if** $S_{new} \notin hypercubes$ **then** ▷ *If recently added candidates to the archive are located outside the hypercubes*
28:    *Update grids to cover* S_{new}
29:   **end if**
30:   *Update* X_α, X_β *and* X_δ
31: **end while**
32: **return** $archive, \hat{P}^{WEC}, \hat{\sigma}_{\bar{q}_1^{nac}}$ ▷ *Pareto-front*
33: **end procedure**

By understanding the characteristics of the objective function's landscape, optimisation algorithms can be designed or tailored to explore or exploit the landscape features better. Landscape analysis is particularly useful for optimisation problems that are non-convex and
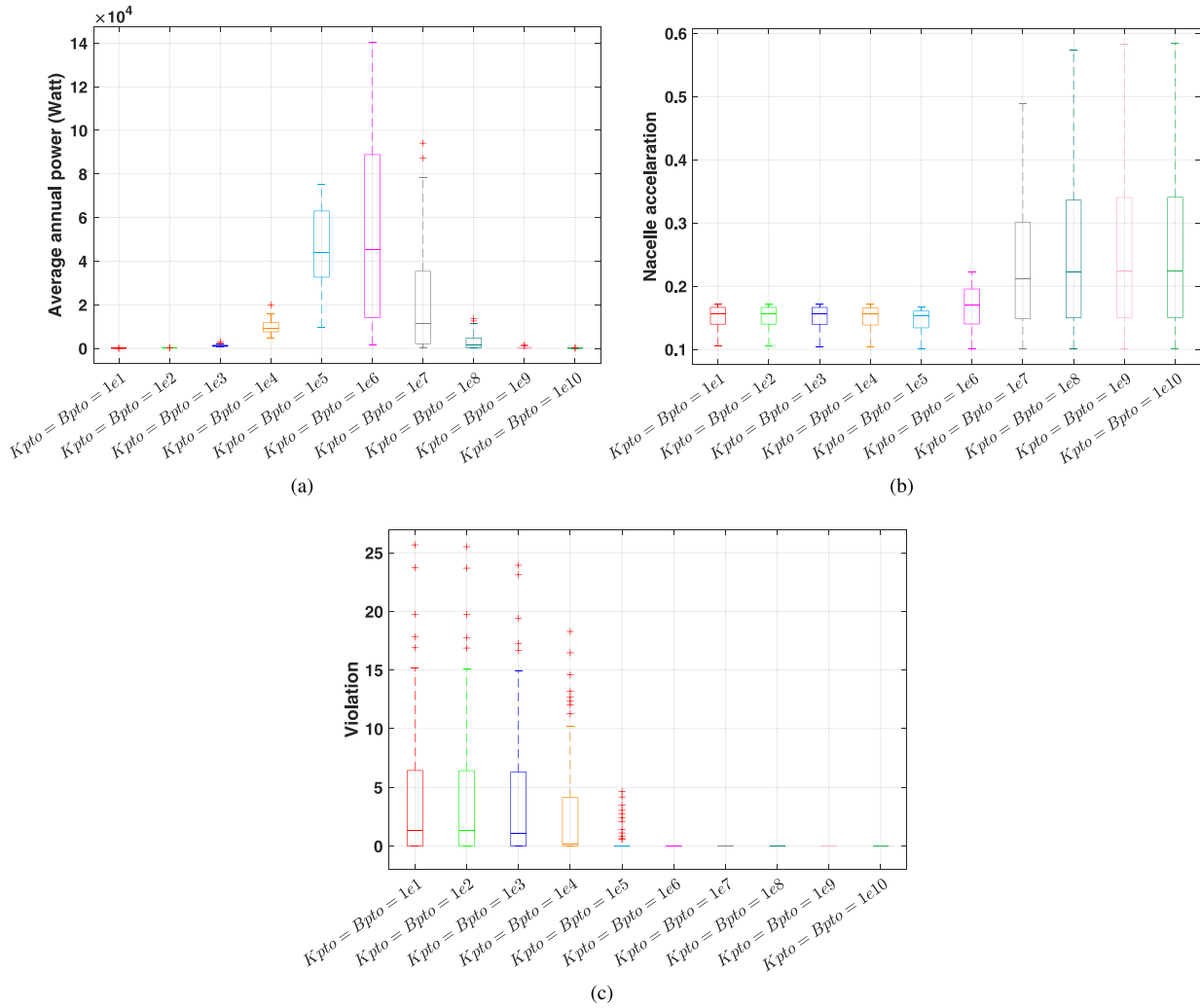
(a)

(b)

(c)

Fig. 11. Statistical analysis of (a) power output, (b) nacelle acceleration of wind turbine, (c) sum violation of allowable displacement based on the Sydney sea site, ($K_{pto} = B_{pto}$). The radius and draught of the hybrid model are set $\{5 \leq r^{WEC} \leq 10\}$ and $\{5 \leq H^{WEC} \leq 15\}$. Therefore, each box shows the distribution of all combinations of radius and height.

high-dimensional, where there may be multiple local optima, and the global optimum is challenging to locate.

In this regard, we use the grid search method to implement a simple landscape analysis of the hybrid wave-wind model and investigate the impact of both damping (K_{pto}) and spring (B_{pto}) PTO parameters combined with the radius of the WECs and draught, their distance from the floating wind turbine. Fig. 11 shows the statistical results of absorbed power output, wind turbine nacelle acceleration and the violation occurred by the unallowable displacements of floating WECs. To simplify the model, we assume the same K_{pto} and B_{pto} values. Fig. 11 shows that the highest power output may be obtained with $K_{pto} = B_{pto} = 1.0E + 5$. However, this range of PTO values makes a considerable level of violation (< 5). To have the minimum violation and infeasible configurations where both K_{pto} and B_{pto} parameters are equal, we recommend using the PTO coefficients greater than $1.0E + 6$. In contrast with statistical violation distribution, the best nacelle acceleration results observed for K_{pto} and B_{pto} are less than $1.0E + 5$.

In the landscape analysis conducted on hybrid wave-wind systems, we evaluated the model's performance by examining the feasible WEC's range of radius and draught along with predefined values of K_{pto} and B_{pto}, as depicted in Fig. 12(a) and (b). The key finding of utmost significance revealed that the optimal size of the WEC's radius and draught is less than seven, enabling efficient power absorption, as illustrated in Fig. 12(c). It is noteworthy that all ten values of K_{pto}, as well as B_{pto}, were assumed to be identical. However, we observed

that the optimal ranges for minimising nacelle acceleration differ considerably, as evidenced in Fig. 12(d). This conflicting behaviour serves as a compelling motivation for treating this optimisation problem as a multi-objective concept. Additionally, Fig. 12(e) visually represents the feasible (dark blue) and infeasible ranges of radius and draught, thereby establishing the presence of a constraint optimisation problem.

To investigate the influence of different PTO configuration values, we conducted a comprehensive landscape analysis of the radius and draught parameters in conjunction with various PTO values, namely 1.0e3, 1.0e5, 1.0e6, and 1.0e9. Fig. 13 presents the outcomes of this analysis. Notably, the optimal range of radius and draught for maximising power output strongly depends on the PTO values. Precisely, as the PTO values increase, the optimal radius size shifts from five to ten while the optimal draught range decreases to its minimum value. Turning attention to the nacelle acceleration landscape, depicted in the second column of Fig. 13, it becomes evident that lower PTO values (e.g., 1.0e3 and 1.0e5) generate multi-modal and complex search landscapes. In these cases, the optimal radius range lies between nine and ten, while it extends above ten for draught. Similar to the power landscape observations, increasing PTO values shifts the optimal draught zone towards smaller values. Finally, the violation landscape, presented in the third column of Fig. 13, confirms our expectations. All configurations of radius and draught yield feasible fitness values for PTO parameters greater than 1.0e5. However, for lower PTO values, violations are observed in cases where the draught exceeds 12. In summary, these
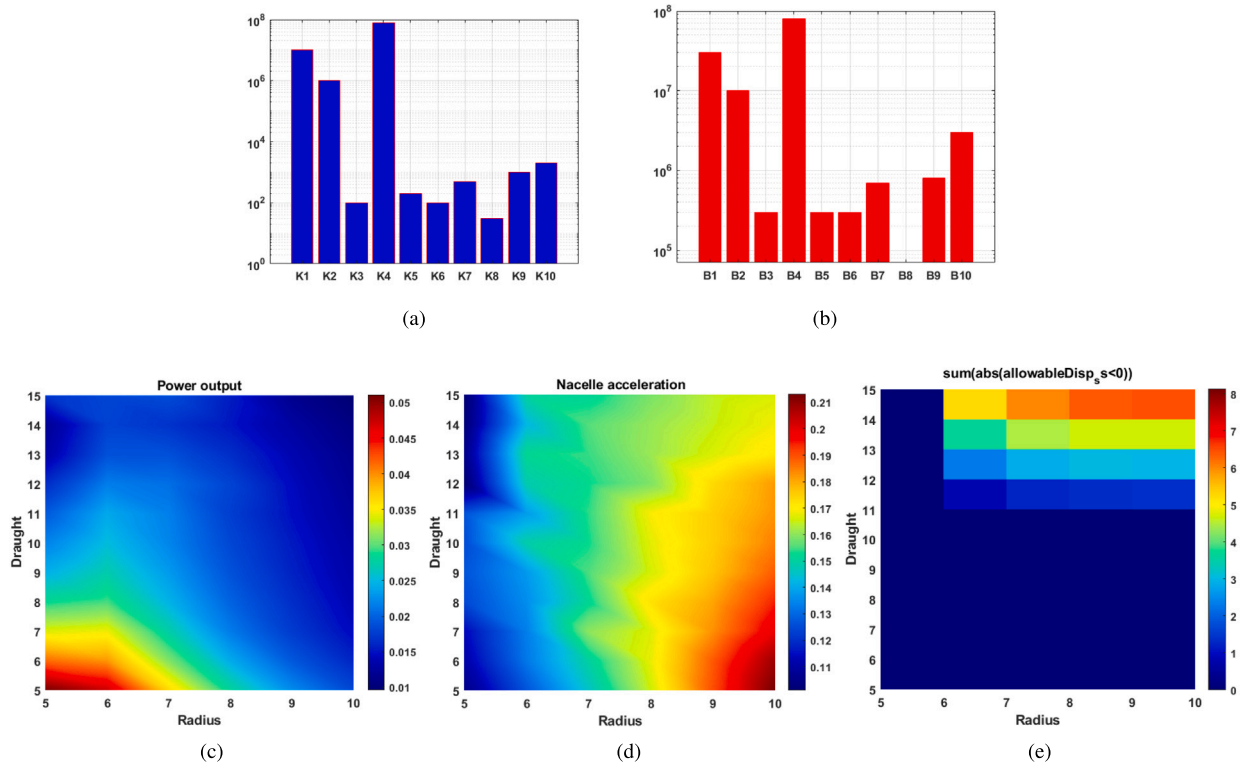
Fig. 12. Landscape analysis of the hybrid wave-wind model: (a) spring coefficient of PTO, (b) damping coefficient of PTO, (c) hybrid power output factor (should be maximised), (d) nacelle acceleration of wind turbine (should be minimised), (d) sum violation of allowable displacement.

experimental analyses highlight the intricate and nonlinear relationship between PTO parameters and the radius and draught.

5.2. Hypervolume comparison

In multi-objective optimisation, the hypervolume indicator is a performance metric that measures the quality of a set of solutions, also known as a Pareto front or Pareto set, regarding its coverage of the objective space. The objective space is the multi-dimensional space defined by the values of the objective functions that are being optimised. The hypervolume indicator calculates the volume of the objective space dominated by the set of solutions being evaluated.

The hypervolume indicator is defined as the volume of the objective space that is dominated by the set of solutions being evaluated and is bounded by a reference point, which is typically set to be the origin of the objective space [91]. The hypervolume indicator is a widely utilised metric in multi-objective optimisation due to its assortment of desirable attributes. It possesses the capability of being easily computed, adaptable to high-dimensional issues, and responsive to both the convergence and diversity of the set of solutions. Furthermore, it presents a valuable comparative metric for varied solutions or alternative algorithms. In order to compute the hypervolume indicator, it is customary to initially aggregate the hypervolume contribution of each solution within the set. This contribution refers to the volume of the objective space dominated by the respective solution and bounded by the reference point. Subsequently, the hypervolume contribution of each solution is summed to derive the overall hypervolume of the solution set. The higher the hypervolume, the more favourable the solution is set.

Fig. 14 indicates that the relatively best-performed multi-objective methods are MOPSO and MOGWA in terms of the maximum hypervolume of the Pareto front compared with other optimisation algorithms. Moreover, SPEA-II performance is competitive and robust, with the minimum STD for ten independent runs. MODA shows the lowest

performance among all methods considered in this study. Furthermore, MOEAD is not as robust as other methods as it shows a wide spread in the calculated Hypervolume. Other methods show a similar performance with a small STD.

5.3. Convergence speed comparison

For several reasons, the convergence rate plays a crucial role in evaluating multi-objective optimisation (MOO) methods. Firstly, it offers valuable insights into the efficacy of optimisation methods in navigating the search space and enhancing the quality of the best solutions discovered throughout the iterations [92]. A higher convergence rate signifies the ability of a method to rapidly approach nearly optimal solutions, thereby demonstrating its efficiency in exploring the objective space. Additionally, the convergence rate enables a fair comparison of optimisation methods, especially when considering the constraints of computational resources. MOO methods often operate within limited computational budgets, and evaluating them based on the number of iterations may be challenging. In such scenarios, the convergence rate becomes an invaluable metric as it quantifies the rate of improvement in objective values within a predetermined number of iterations or computational budget, making it a suitable criterion for comparison. By assessing the convergence rate, researchers and practitioners can evaluate the efficiency and effectiveness of various MOO methods in achieving desirable solutions within a given computational budget. This metric provides a quantitative measure of the performance of these methods in terms of solution quality and the trade-off between exploration and exploitation, thereby facilitating informed decision-making in selecting an appropriate MOO method for a specific problem.

Furthermore, the performance of optimisation evolutionary-based algorithms can exhibit fluctuations during each execution due to the stochastic characteristics of the elements engaged. By conducting multiple iterations of the algorithms, one can observe the fluctuation in performance and evaluate the algorithm's robustness and stability.
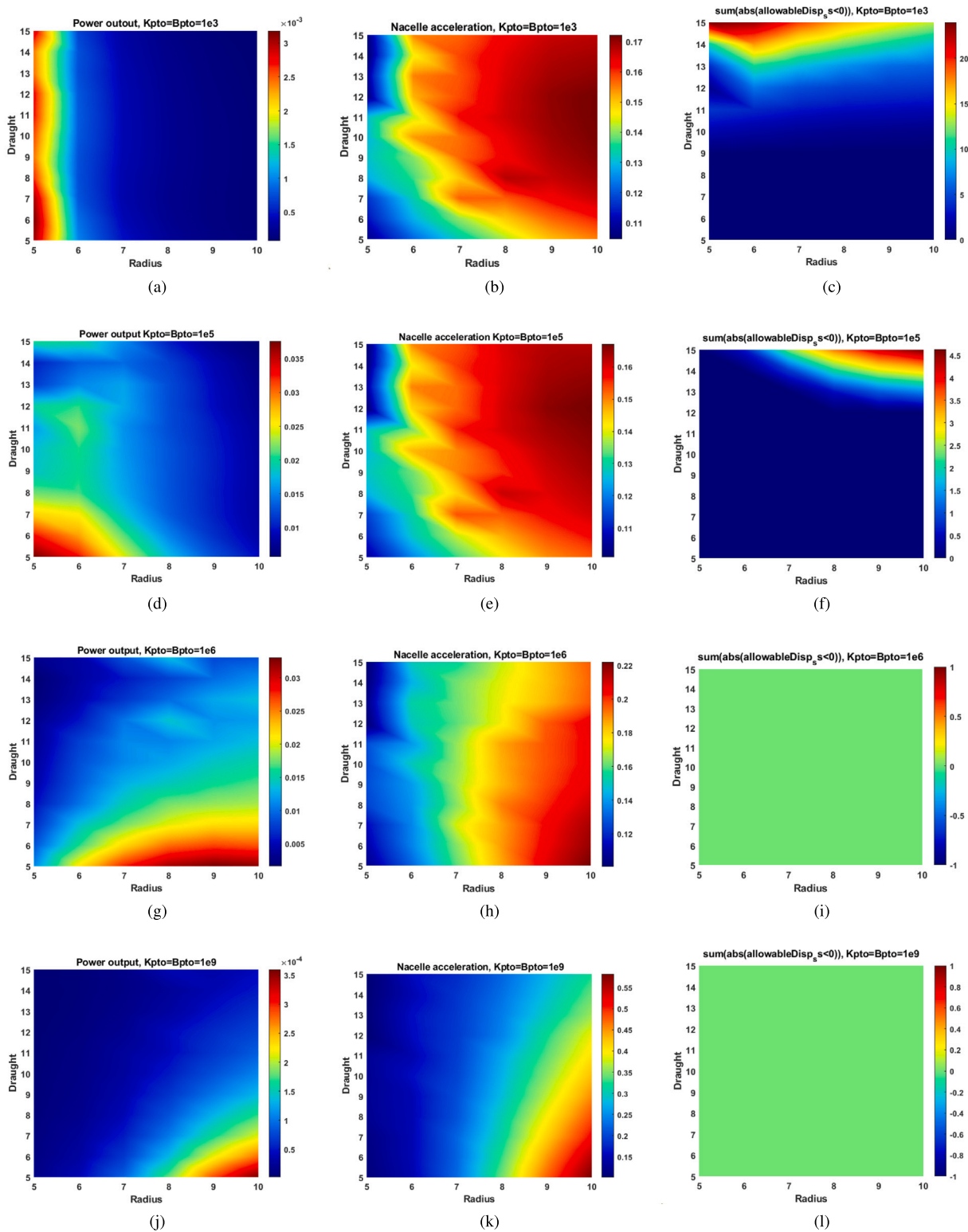
Fig. 13. Landscape analysis of the hybrid wave-wind model: first column, hybrid power output factor (should be maximised), second column, the nacelle acceleration of wind turbine that should be minimised, and third column is the sum violation of allowable displacement.

Running the algorithms multiple times can furnish a more exhaustive comprehension of the behavioural patterns and effectiveness of the algorithm. In this regard, we demonstrate the WECs power output convergence speed of eight multi-objective optimisation methods with a standard deviation shadow of ten runs that can be seen in Fig. 15. This figure shows that most of the algorithms are fully converged,

and extending the runtime cannot improve the Pareto front, except for NSGA-II. Secondly, the best solutions found by CMOGWA and DMOGWA proposed the highest WEC power output compared with others. In terms of robustness through ten runs, DMOGWA demonstrated a high level of stability against the random behaviour of the other methods.

Table 8
Statistical details of Bi-objective optimisation of the hybrid wave-wind converter model using eight multi-objective optimisation methods based on the Sydney sea site.

|	WEC annual power									
	MODA	MOEAD	MALO	MOGWA	MOPSO	NSGA-II	PESA-II	SPEA-II	CMOGWA	DMOGWA
Min	1.600E+02	4.906E+01	4.288E+03	1.125E+04	1.133E+03	5.061E+02	5.713E+03	4.778E+03	3.286E+04	5.638E+04
Max	2.174E+02	3.282E+03	3.353E+04	1.443E+05	4.287E+04	2.325E+04	1.970E+04	2.315E+04	1.908E+05	2.053E+05
Mean	1.866E+02	1.134E+03	1.373E+04	8.779E+04	1.390E+04	1.061E+04	1.012E+04	1.565E+04	1.040E+05	**1.193E+05**
Median	1.853E+02	6.468E+02	1.033E+04	9.565E+04	7.362E+03	9.778E+03	7.710E+03	1.740E+04	8.472E+04	1.018E+05
STD	1.750E+01	1.221E+03	8.794E+03	4.084E+04	1.354E+04	7.347E+03	5.356E+03	6.325E+03	6.049E+04	4.904E+04
	Wind turbine nacelle acceleration									
	MODA	MOEAD	MALO	MOGWA	MOPSO	NSGA-II	PESA-II	SPEA-II	CMOGWA	DMOGWA
Min	2.977E−01	1.004E−01	1.009E−01	1.162E−01	1.082E−01	1.520E−01	1.118E−01	1.174E−01	1.124E−01	1.383E−01
Max	3.243E−01	1.465E−01	1.034E−01	1.865E−01	1.483E−01	2.078E−01	1.235E−01	1.888E−01	1.482E−01	1.653E−01
Mean	3.217E−01	1.171E−01	**1.014E−01**	1.355E−01	1.285E−01	1.710E−01	1.160E−01	1.620E−01	1.239E−01	1.506E−01
Median	3.243E−01	1.045E−01	1.010E−01	1.282E−01	1.265E−01	1.642E−01	1.151E−01	1.713E−01	1.251E−01	1.479E−01
STD	8.427E−03	1.975E−02	8.147E−04	2.100E−02	1.265E−02	1.794E−02	3.719E−03	2.144E−02	9.971E−03	9.941E−03
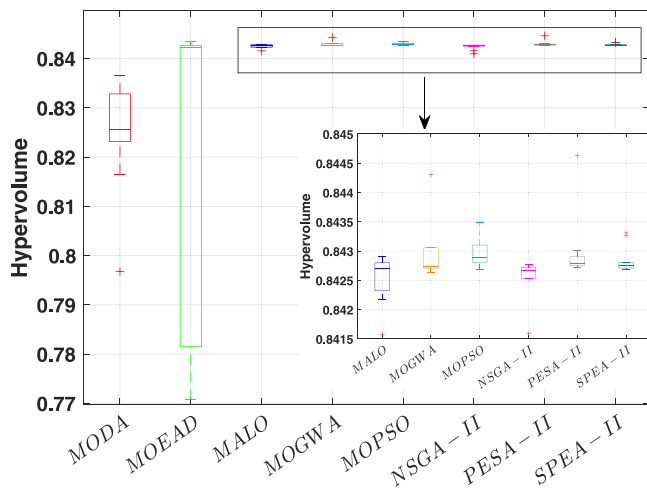
Fig. 14. Hypervolumes covered by the final populations of eight multi-objective optimisation algorithms in Sydney sea site.

To support the convergence rate observations, Tables 8, 9, 10, and 11 report the statistical results of best-found configurations of the proposed method compared with eight other well-known multi-objective optimisation methods for the average power output and nacelle acceleration of wind turbines in Sydney, Port Lincoln, Gippsland, and Cliff Head sea site, respectively. It is crystal clear that the proposed method (DMOGWA) considerably outperforms all other methods in terms of the absorbed power output of WECs in four sea sites. However, in order to minimise nacelle acceleration in the Sydney site, MALO and PESA-II perform better and find solutions with lower coefficients (1.014E−01 and 1.16E−01) than DMOGWA.

The comparative optimisation results for the Port Lincoln sea site are presented in Table 9. Regarding average WEC annual power, the most effective method is DMOGWA, exhibiting power improvements of 80.2%, 98.9%, and 243.2% compared to CMOGWA, MOGWA, and MOPSO, respectively. Conversely, in the context of minimising wind turbine nacelle acceleration, MOEAD demonstrates superior performance, surpassing DMOGWA by a margin of 24.79%, securing the top rank among other multi-objective optimisation methods. The superior performance of MOEAD in minimising nacelle acceleration may be attributed to its emphasis on exploration through the decomposition of the multi-objective problem into subproblems and their subsequent optimisation. This decomposition approach enables MOEAD to explore a wide range of solutions throughout the objective space, facilitating the discovery of diverse and promising solutions. Conversely, MOGWA, a population-based algorithm inspired by particle social behaviour,

exhibits a stronger tendency towards exploitation, concentrating on refining and enhancing the current population of solutions. In situations where exploration plays a critical role, MOEAD's exploration-oriented strategy proves advantageous, leading to improved performance in specific objectives.

In the sea sites of Gippsland and Cliff Head, the proposed optimisation method, DMOGWA, exhibited significant superiority over two other variants of the GWO, MOPSO and other evolutionary-based methods. This superiority was observed in two objectives: maximising the annual power of the WEC and minimising the nacelle acceleration. Detailed results can be found in Table 10 and 11.

When it comes to optimising the total power of WEC according to the results in Table 10, the performance of the DMOGWA stands out, surpassing both the MOGWA and the MOPSO approaches. DMOGWA exhibits remarkable advancement, achieving a power increase of 330% and 372% compared to MOGWA and MOPSO, respectively. The notable enhancement in DMOGWA's performance can be attributed to several factors. Firstly, a key element is the incorporation of a chaotic sequence, which is mapped through a normalising function. This mapping process ensures a delicate balance between exploitation and exploration, promoting stability within the optimisation process. This equilibrium allows DMOGWA to navigate the search space efficiently, effectively identifying optimal solutions. Besides, DMOGWA utilises a discretisation technique that plays a crucial role in achieving superior results. Continuous PTO parameters are transformed into a discretised space by employing the logarithm function with a base of 10. This technique effectively reduces the dimensionality of the search space, simplifying the optimisation problem. Consequently, the number of feasible solutions is confined, enabling DMOGWA to focus its search on specific regions of interest. This targeted approach enhances the algorithm's efficiency and effectiveness, leading to improved performance in power optimisation for WECs.

To develop a fair comparative framework and evaluate the efficiency of the proposed method, we run all multi-objective optimisation methods with the same population size and iteration. Fig. 16 indicates the convergence of average WECs power out (part a) and a comparison between DMOGWA, CMOGWA and standard MOGWA (part b) of the best configuration over time for the whole of the methods. As can be seen in Fig. 16, DMOGWA and CMOGWA converged rapidly, yielding designs that exhibit high power outputs and consistently outperform the other techniques. Notably, Fig. 16(b) reveals an intriguing and significant observation: DMOGWA initiates the optimisation process with a higher level of configuration power. This outcome is primarily attributed to the Discretisation strategy, which ensures a balanced distribution of PTO parameters within the initial population (as depicted in Fig. 10). On the other hand, in Fig. 17 MOEAD and PESA-II quickly converged into the local optimum of the nacelle coefficient with low values (less than 0.15) in the initial 500 evaluation numbers and
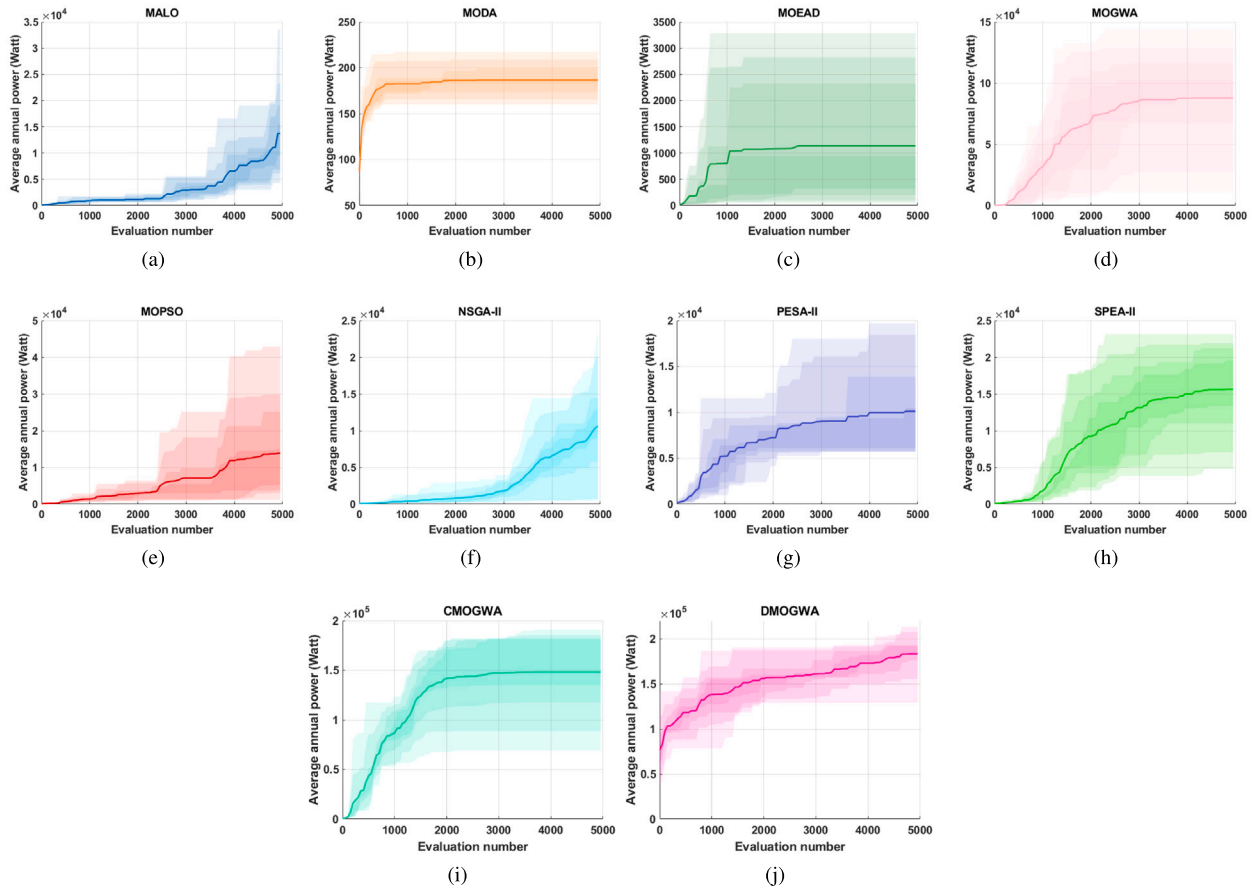
Fig. 15. The optimisation convergence rate for ten multi-objective optimisation methods based on the Sydney sea site. The main line shows the average performance of each generation. Each method runs ten times independently, with different random solutions generated in the initial generation.

Table 9
Statistical details of the hybrid wave-wind model using the proposed and nine popular multi-objective optimisation methods based on the Port Lincoln sea site.

	MODA	MOEAD	MALO	MOGWA	MOPSO	NSGA-II	PESA-II	SPEA-II	CMOGWA	DMOGWA
					WEC annual power					
Min	1.187E+03	2.982E+02	7.444E+02	1.038E+04	4.590E+04	2.545E+04	1.520E+04	1.175E+04	4.725E+04	2.003E+05
Max	4.658E+03	5.734E+03	4.695E+04	2.191E+05	1.402E+05	5.958E+04	5.043E+04	7.119E+04	2.191E+05	3.569E+05
Mean	2.193E+03	3.511E+03	1.407E+04	1.415E+05	8.204E+04	3.668E+04	3.400E+04	3.919E+04	1.561E+05	**2.815E+05**
Median	1.930E+03	3.489E+03	7.459E+03	1.546E+05	7.606E+04	3.397E+04	3.775E+04	4.006E+04	1.739E+05	2.817E+05
STD	1.009E+03	1.789E+03	1.679E+04	7.535E+04	3.487E+04	1.025E+04	1.203E+04	2.094E+04	6.324E+04	5.727E+04
					Wind turbine nacelle acceleration					
	MODA	MOEAD	MALO	MOGWA	MOPSO	NSGA-II	PESA-II	SPEA-II	CMOGWA	DMOGWA
Min	4.853E−01	6.509E−02	6.528E−02	1.161E−01	1.114E−01	1.961E−01	8.728E−02	8.264E−02	1.161E−01	9.512E−02
Max	7.353E−01	1.799E−01	5.240E−01	3.831E−01	4.793E−01	5.150E−01	4.351E−01	4.029E−01	2.674E−01	1.961E−01
Mean	7.012E−01	**1.098E−01**	2.225E−01	2.151E−01	2.678E−01	2.956E−01	2.585E−01	2.779E−01	1.965E−01	1.460E−01
Median	7.352E−01	6.558E−02	1.696E−01	2.077E−01	2.380E−01	2.847E−01	2.392E−01	2.913E−01	2.007E−01	1.468E−01
STD	7.821E−02	5.756E−02	1.510E−01	7.388E−02	1.043E−01	9.888E−02	9.879E−02	9.908E−02	4.717E−02	2.822E−02

outperformed others; however, MALO searchability could surpass both MOEAD and PESA-II after 1000 evaluation number.

To expand our evaluation of the proposed multi-objective optimisation method (DMOGWA), we compared it with nine well-known methods that use different algorithms and strategies to balance two conflicting objectives at the Cliff Head sea site. Among the ten techniques, DMOGWA emerged as the clear leader in terms of convergence speed in maximising the average power of WEC (as shown in Fig. 18(a)). DMOGWA demonstrated an impressive ability to converge

to feasible solutions with high power output from the WEC, making it highly effective in finding a trade-off between maximising power generation and minimising nacelle acceleration. This also means DMOGWA can help maintain the structural integrity of the wind turbine.

Furthermore, Fig. 18(a) shows that CMOGWA, while not as robust as DMOGWA, still performed well and had the second-best convergence rate. CMOGWA's ability to converge to near-optimal solutions relatively quickly indicates it has the potential for achieving a favourable balance between power generation and nacelle acceleration.

Table 10
The hybrid wave-wind model optimisation results using the proposed and nine popular multi-objective optimisation methods based on the Gippsland sea site.

				WEC annual power						
	MODA	MOEAD	MALO	MOGWA	MOPSO	NSGA-II	PESA-II	SPEA-II	CMOGWA	DMOGWA
Min	8.612E+01	1.520E+02	2.407E+01	6.968E+02	1.747E+03	3.077E+02	8.032E+02	1.534E+03	1.052E+03	2.317E+04
Max	2.958E+02	2.870E+03	9.296E+03	1.697E+04	1.243E+04	6.665E+03	1.208E+04	8.979E+03	1.697E+04	3.599E+04
Mean	1.549E+02	8.907E+02	3.012E+03	6.456E+03	5.896E+03	2.583E+03	4.561E+03	4.485E+03	7.096E+03	**2.782E+04**
Median	1.528E+02	6.329E+02	1.994E+03	3.970E+03	5.173E+03	2.264E+03	3.670E+03	3.787E+03	4.118E+03	2.742E+04
STD	6.079E+01	8.452E+02	3.119E+03	5.806E+03	3.177E+03	1.799E+03	3.633E+03	2.594E+03	5.772E+03	3.933E+03
				Wind turbine nacelle acceleration						
	MODA	MOEAD	MALO	MOGWA	MOPSO	NSGA-II	PESA-II	SPEA-II	CMOGWA	DMOGWA
Min	1.620E−01	8.475E−02	6.191E−02	8.096E−02	6.636E−02	6.327E−02	7.486E−02	7.990E−02	8.096E−02	7.792E−02
Max	2.018E−01	1.193E−01	1.794E−01	1.802E−01	1.364E−01	1.871E−01	1.479E−01	1.798E−01	1.762E−01	1.119E−01
Mean	1.978E−01	9.771E−02	1.071E−01	1.158E−01	9.582E−02	1.134E−01	1.102E−01	1.204E−01	1.086E−01	**8.837E−02**
Median	2.017E−01	9.391E−02	1.045E−01	9.812E−02	8.665E−02	1.141E−01	1.105E−01	1.198E−01	9.682E−02	8.715E−02
STD	1.258E−02	1.050E−02	3.181E−02	3.757E−02	2.308E−02	3.301E−02	2.217E−02	2.974E−02	3.182E−02	9.261E−03

Table 11
The hybrid wave-wind model optimisation results using the proposed and nine popular multi-objective optimisation methods based on the Cliff Head sea site.

|				WEC annual power						
	MODA	MOEAD	MALO	MOGWA	MOPSO	NSGA-II	PESA-II	SPEA-II	CMOGWA	DMOGWA
Min	7.511E+02	1.158E+02	9.971E+01	3.663E+02	3.352E+04	2.355E+04	1.461E+04	8.955E+03	1.364E+03	1.232E+05
Max	2.019E+03	3.838E+03	1.211E+05	2.032E+05	1.054E+05	5.012E+04	5.597E+04	6.506E+04	2.032E+05	2.254E+05
Mean	1.106E+03	2.220E+03	1.991E+04	8.791E+04	6.933E+04	3.398E+04	3.164E+04	2.849E+04	9.764E+04	**1.671E+05**
Median	9.790E+02	2.717E+03	2.084E+03	8.384E+04	7.110E+04	3.261E+04	3.116E+04	2.707E+04	9.751E+04	1.547E+05
STD	3.935E+02	1.421E+03	3.765E+04	6.392E+04	2.519E+04	9.555E+03	1.350E+04	1.519E+04	5.943E+04	4.159E+04
				Wind turbine nacelle acceleration						
	MODA	MOEAD	MALO	MOGWA	MOPSO	NSGA-II	PESA-II	SPEA-II	CMOGWA	DMOGWA
Min	4.225E−01	5.476E−02	5.461E−02	1.379E−01	7.731E−02	1.244E−01	9.413E−02	1.029E−01	1.379E−01	9.373E−02
Max	6.197E−01	1.659E−01	5.031E−01	3.663E−01	2.695E−01	3.519E−01	3.305E−01	3.550E−01	3.663E−01	1.427E−01
Mean	5.943E−01	1.154E−01	2.392E−01	2.104E−01	1.991E−01	2.564E−01	1.940E−01	2.387E−01	1.994E−01	1.134E−01
Median	6.197E−01	1.464E−01	2.270E−01	1.826E−01	2.085E−01	2.585E−01	1.916E−01	2.440E−01	1.647E−01	**1.113E−01**
STD	6.151E−02	5.044E−02	1.282E−01	7.620E−02	5.920E−02	7.350E−02	7.694E−02	7.467E−02	7.205E−02	1.603E−02
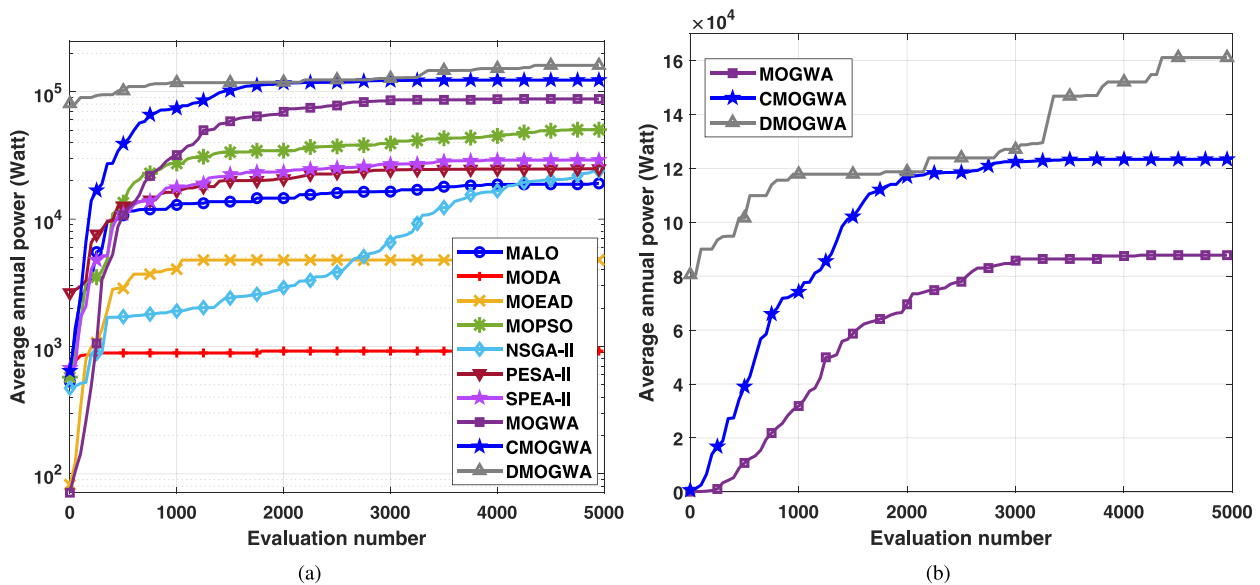
Fig. 16. The convergence rate of the average best-so-far solution's (a) power output of three WECs obtained (should be maximised) by nine multi-objective optimisation algorithms and (b) the proposed method (CMOGWA and DMOGWA) based on the best-found solution so far for each generation in Sydney sea site.

In contrast, MOPSO lagged behind the other three methods regarding convergence performance, showing slower convergence and less impressive results regarding power generation and nacelle acceleration minimisation. However, it is important to note that MOPSO may still have unique strengths or characteristics applicable in specific contexts. Further investigation is necessary to understand its potential fully.

To gain a comparative understanding of the convergence rates of ten optimisation methods in minimising the nacelle acceleration parameter,

we conducted a comprehensive experiment consisting of ten independent runs for each optimiser. The results of this experiment are depicted in Fig. 18(b). Upon analysing the figure, it becomes evident that the MOEAD method exhibited the most rapid convergence speed during the initial 1000 evaluations. However, it struggled to improve the Pareto front effectively as the optimisation progressed. While MOEAD showed promising early performance, it eventually failed to achieve optimal solutions and may converge to a local optimum. In contrast, the
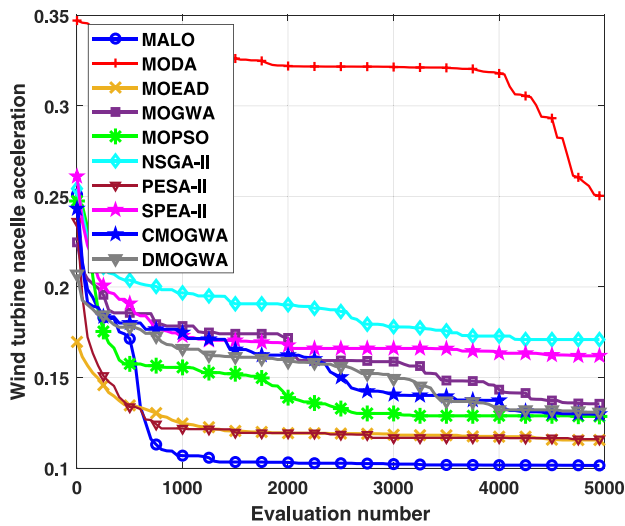
Fig. 17. The convergence rate of the average best-so-far solution's wind turbine nacelle acceleration (should be minimised) by eight multi-objective optimisation algorithms and the proposed method (CMOGWA and DMOGWA) based on the best-found solution so far for each generation in Sydney sea site.

DMOGWA optimiser emerged as the top performer when considering the entire computational budget (See Fig. 18(b)). It consistently outperformed the other nine methods throughout the experiment, showcasing its superiority in finding high-quality solutions. DMOGWA's ability to surpass the competition and yield optimal results demonstrates its effectiveness in minimising the nacelle acceleration parameter. The findings highlight that while MOEAD exhibited rapid initial convergence, it struggled to improve over time. On the other hand, DMOGWA consistently delivered exceptional results and outperformed its counterparts.

Fig. 19 presents the box-and-whisker plots depicting the performance comparison of ten multi-objective optimisation methods in optimising the total absorbed power across four sea sites. This visualization concisely summarises the optimisation results, capturing central tendency, dispersion, and potential outliers. The plot comprises a box representing the interquartile range (IQR), a line within the box indicating the median, and "whiskers" or lines extending from the box to display the data range. A key observation from the plot is the superior median performance of the DMOGWA compared to other methods. Additionally, the variance performance of DMOGWA stands out when considering the configurations with high power proposed by this method. It is important to note that the comparison scale in the plot is logarithmic, enabling better observation and comparison.

Among the ten optimisation methods evaluated, the second and third best-performing optimisers were CMOGWA and MOPSO, respectively. These optimisers demonstrated commendable performance across various sea sites and wave scenarios. In particular, CMOGWA showcased competitive performance compared to the top-performing DMOGWA method, except for the optimisation results obtained at the Gippsland Sea site. CMOGWA consistently proposed settings with good-quality solutions, indicating its effectiveness in optimising the problem at hand. This observation highlights CMOGWA as a strong contender for achieving high-quality results, making it a promising choice for multiobjective optimisation tasks. Additionally, Fig. 19 revealed an intriguing finding regarding the effectiveness of DMOGWA. Remarkably, DMOGWA displayed high robustness and independence across different sea sites and wave scenarios. It consistently delivered outstanding performance across all four sea sites, underscoring its reliability and efficacy as an optimisation method. This robustness makes DMOGWA a valuable choice for addressing multiobjective optimisation problems in various real-world scenarios.

To facilitate a comprehensive comparison of ten multi-objective optimisation methods in terms of minimising nacelle acceleration, Fig. 20 showcases four boxplots. In the case studies of Gippsland and Cliff Head, the proposed method, DMOGWA, demonstrates a notable level of performance, surpassing other methods with remarkable robustness. Conversely, MOEAD emerges as the best-performing method in the Port Lincoln site, followed by DMOGWA. The optimisation results diverge in the Sydney site, where MALO and PESA-II exhibit desirable effectiveness in minimising nacelle acceleration. These findings highlight the varying performance of the multi-objective optimisation methods across different study sites, underscoring the importance of tailoring the method selection to each site's specific characteristics and requirements.

5.4. Pareto front coverage and solutions

As we are faced with a bi-objective optimisation problem, having a landscape of all the best-found feasible solutions proposed by nine methods can be helpful. Pareto front coverage serves as an evaluative measure that measures the effectiveness of a multi-objective optimisation technique in approximating the Pareto front. The Pareto front represents the optimal set of solutions in the objective space, where enhancing one objective comes at the cost of deteriorating at least one other objective. To assess the Pareto front coverage, the solutions generated by the technique are compared to the actual Pareto front if it is already known or obtainable through alternative means, such as a reference set of solutions. This metric quantifies the degree to which the solutions encompass the Pareto front and how well they capture its shape and distribution. A technique that demonstrates superior Pareto front coverage produces various solutions spanning the Pareto front, comprehensively capturing the trade-offs. This implies that the method has the capacity to generate solutions that represent a wide range of objective combinations, thereby providing decision-makers with an extensive selection of trade-off options.

Fig. 21 shows the Pareto front and solution distribution of the last population for all procedures, and a zoomed version is shown on the right side. The most important observation of Fig. 21(b) is that the proposed method (CMOGWA) could find several feasible solutions with a high level of power output combined with low nacelle acceleration values. These Pareto front observations support the considerable performance of CMOGWA compared with other optimisation methods.

Fig. 22 indicates that DMOGWA exhibits remarkable convergence and coverage capabilities when optimising the performance of the hybrid platform across the four sea sites in both objectives. Moving forward, upon careful examination of Fig. 22, it becomes evident that DMOGWA consistently demonstrates fewer values and a narrower distribution of the IGD metric in most cases. This observation highlights the significant superiority of DMOGWA when compared to state-of-the-art MOEAs.

The primary benefit of the adaptive chaotic control search step is that it empowers DMOGWA to dynamically modify the step size, taking into account the intricate nature of the fitness landscape and the current state of the search. By infusing the algorithm with chaotic behaviour, it becomes capable of delving into the vast solution space with more remarkable thoroughness during the initial optimisation stages, all the while honing in on exploitation and convergence as the optimisation progresses. This delicate balance between exploration and exploitation serves as a guiding light for DMOGWA, enabling it to efficiently explore the most optimal Pareto solutions with immense precision and finesse.

Fig. 23 shows parallel coordinates of the correlation among various parameters involved in optimising the WEC power. The plot effectively represents the influence of radius, draught, ten values of K_{PTO}, ten values of B_{PTO}, and the subsequent power output of the WEC. Each vertical axis within the plot corresponds to a distinct parameter, with the data points being interconnected by lines, forming a collection of parallel lines. The position of each data point on each axis represents
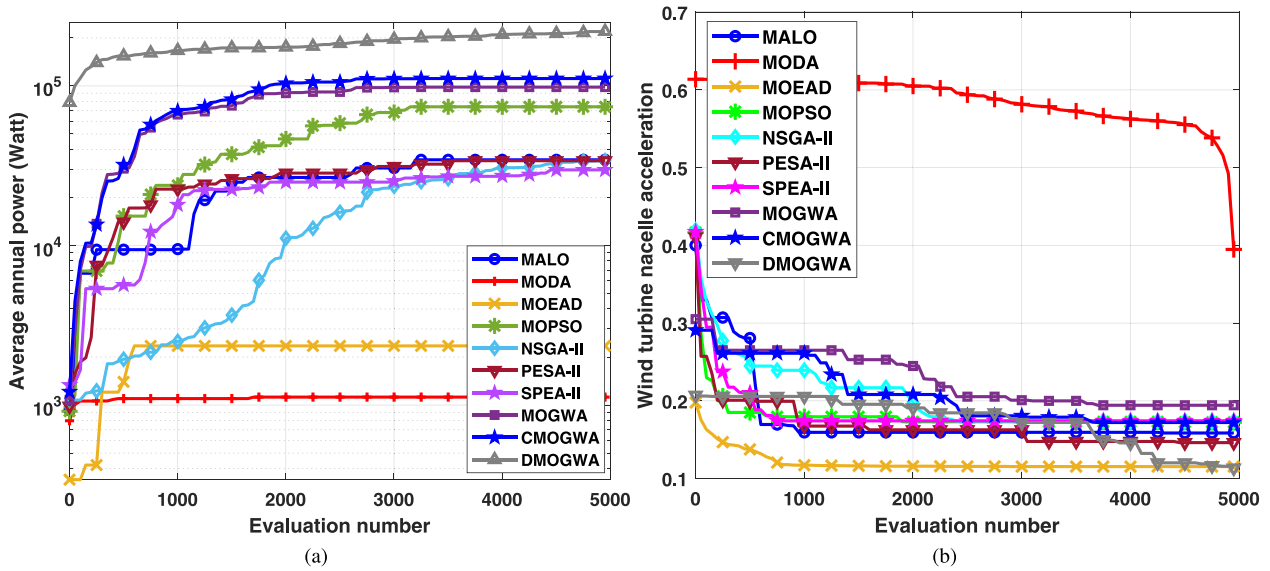
Fig. 18. The convergence rate of the average best-so-far solution's (a) power output of three WECs obtained (should be maximised) by nine multi-objective optimisation algorithms and (b) wind turbine nacelle acceleration (should be minimised) in Cliff Head sea site.
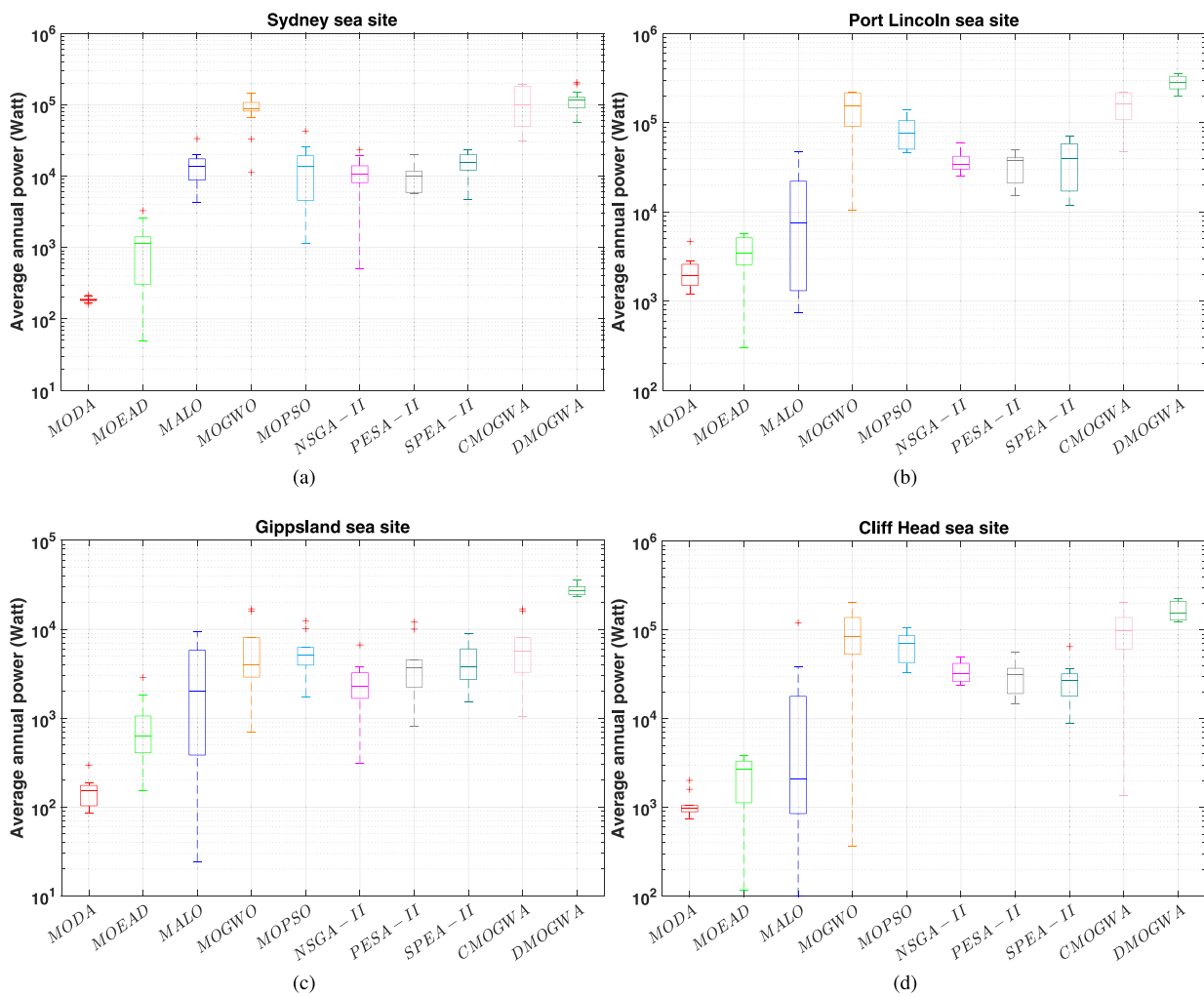

Fig. 19. (a) The optimisation of average annual power output with considering minimising nacelle acceleration for ten multi-objective optimisation methods. Each method runs ten times independently, with different random solutions generated in the initial iteration.
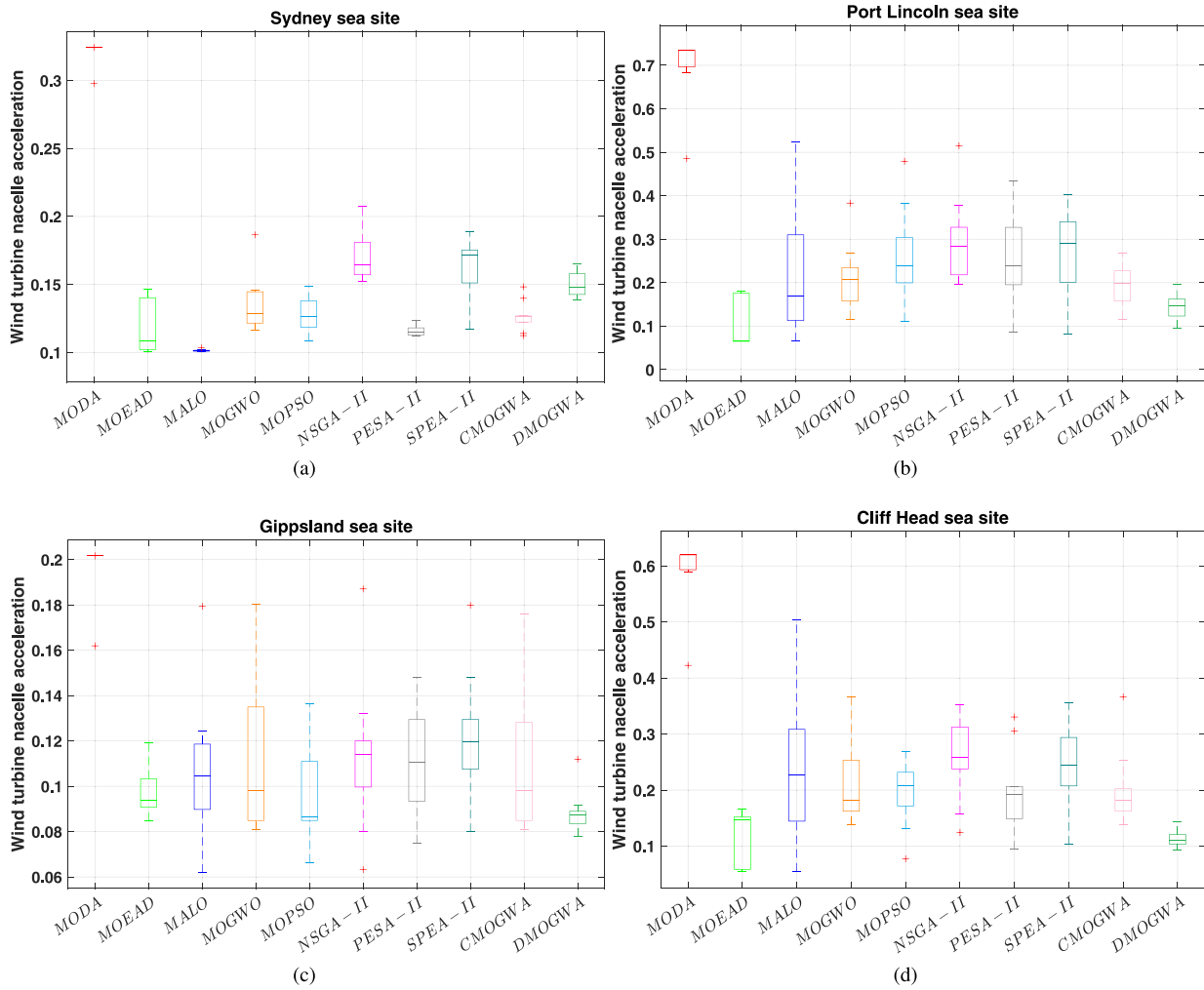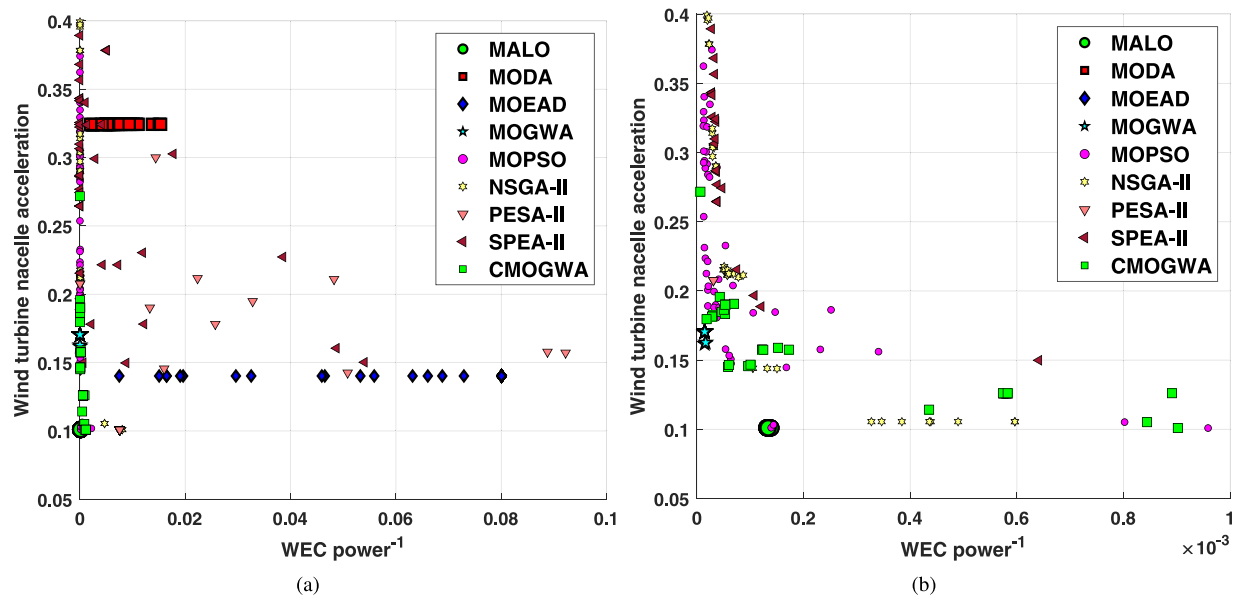
Fig. 20. The optimisation of average nacelle acceleration (minimising) with considering maximising average power output of WECs for ten multi-objective optimisation methods. Each method runs ten times independently, with different random solutions generated in the initial iteration.

Fig. 21. The Pareto front and Pareto solution distribution of the last generation proposed by eight multi-objective optimisation methods.
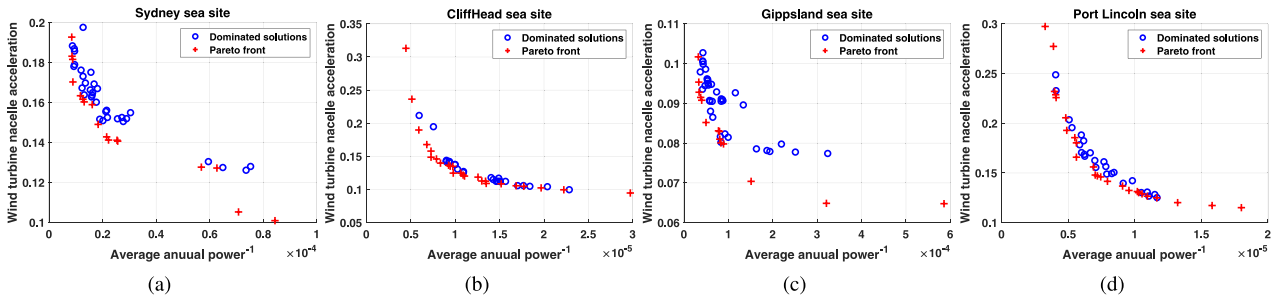
Fig. 22. The Pareto front and dominated solutions distribution of the last generation proposed by DMOGEA.
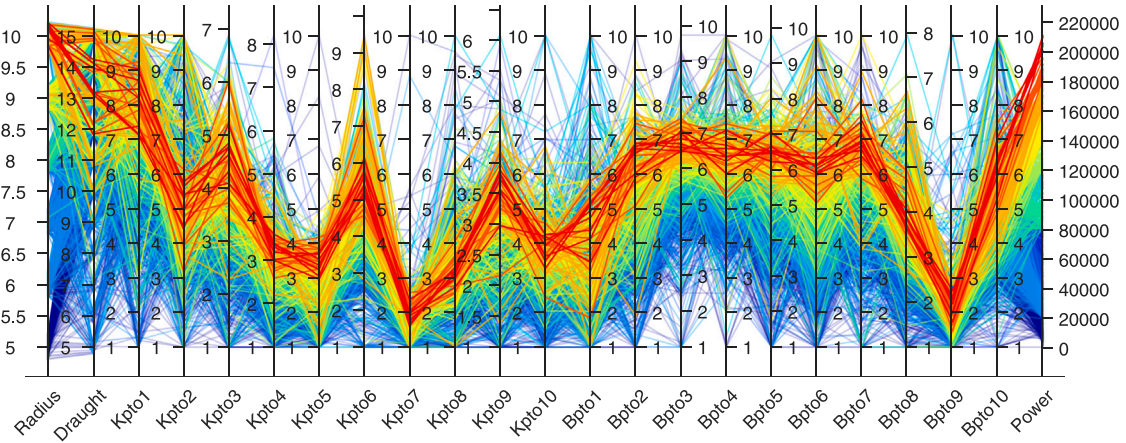

Fig. 23. Parallel coordinates plot of WEC power optimisation parameters for all iterations Pareto-front of DMOGWO based on the Cliff Head site. It is noted that the values of K_{pto} and B_{pto} are computed by a log function as 10^{PTO}.

the corresponding parameter's value. The plot offers a comprehensive perspective on how modifications in one parameter impact the others and, ultimately, the power output of the WEC. The application of parallel coordinates permits a visual examination of the relationships between the parameters. By evaluating the convergence or divergence of the lines across the multiple axes, patterns, trends, and trade-offs can be discerned. The plot facilitates the identification of the most favourable combinations of radius, draught, K_{PTO}, and B_{PTO} values that yield the most incredible power output for the WEC.

5.5. Wind-wave system design analysis

The results reported in Section 5.4 can be related to the original optimisation problem on how to design the hybrid wind-wave system and how the WEC radius and draught affect the power production and stability of the floating platform. Using the Sydney site as an example, the results that correspond to the Pareto front in Fig. 21 are re-drawn in Fig. 24 in terms of the corresponding WEC radius and draught. In Fig. 24(a), the marker size is proportional to the WEC power absorption, while the marker colour corresponds to the wind turbine nacelle acceleration. From the wave energy conversion point of view, the power production is expected to increase with increasing WEC radius, and this can be seen in Fig. 24(a). For WECs that absorb power in heave mode only, the role of draught in power generation is less significant, which is also clearly demonstrated in Fig. 24(a) (refer to the same size of markers corresponding to a fixed radius). Similar to the annual average power, the wind turbine nacelle acceleration also strongly depends on the WEC radius but not on the WEC draught. These results are reinforced in Fig. 24(b), demonstrating that larger WECs (regardless of the WEC draught) can generate more power, which always leads to an increase in nacelle acceleration. As a result, the maximum possible amount of power that three torus-shaped WECs can

generate at the Sydney site annually is close to 200 kW, which is less than 10% of the power generated by the 5-MW floating wind turbine.

Similar results but for different potential deployment sites are shown in Fig. 25. The main finding from the Sydney site is that increases in the WEC power and nacelle acceleration are always associated with the increase in WEC radius, which holds for all four deployment sites analysed in this paper. However, the influence of the WEC draught on the performance of the hybrid wind-wave system appears to be site-dependent. A more pronounced effect is observed at the Port Lincoln site (refer to Fig. 25(c)), where larger draughts lead to higher WEC power output. In addition to the WEC design parameters, such as draught and radius, the tuning of the WEC power take-off can also be used to change the performance of the hybrid wind-wave system depending on the environmental conditions. Thus, at the Cliff Head site (see Fig. 25(d)), the WECs with a radius of 10 m (blue circles), and a draught of 15 m, can generate power between 147 and 225 kW with a corresponding nacelle acceleration between 0.16 and 0.35 m/s^2. This range of operating conditions is possible by adjusting the PTO parameters.

The results presented in this paper can be used as a first step towards designing hybrid wind-wave systems. Wave energy converters can increase the annual power production of the floating offshore wind turbine and significantly adjust the dynamics of the floating foundation. However, it is acknowledged that final design decisions are always driven by the reliability, durability, and economic feasibility of the hybrid system.

5.6. Limitations of the proposed multi-objective optimisation method

This section examines various aspects of the limitations of the proposed optimisation method to create opportunities for future improvements as follows.
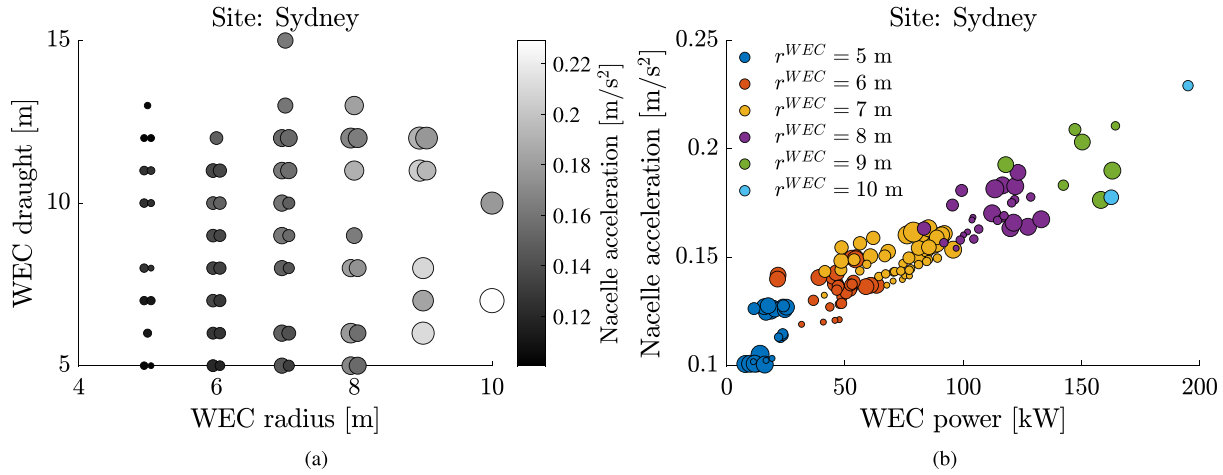
Fig. 24. The dependence of WEC power and wind turbine nacelle acceleration on the WEC radius and draught based on values from Pareto front for the Sydney site: (a) the marker size is proportional to the WEC annual average power production and marker colour corresponds to the wind turbine nacelle acceleration when two markers are shown, one corresponds to the maximisation of the WEC power output, while the second one is related to the minimisation of the nacelle acceleration; (b) marker colours correspond to different WEC radii, while the marker size is proportional to the WEC draught.
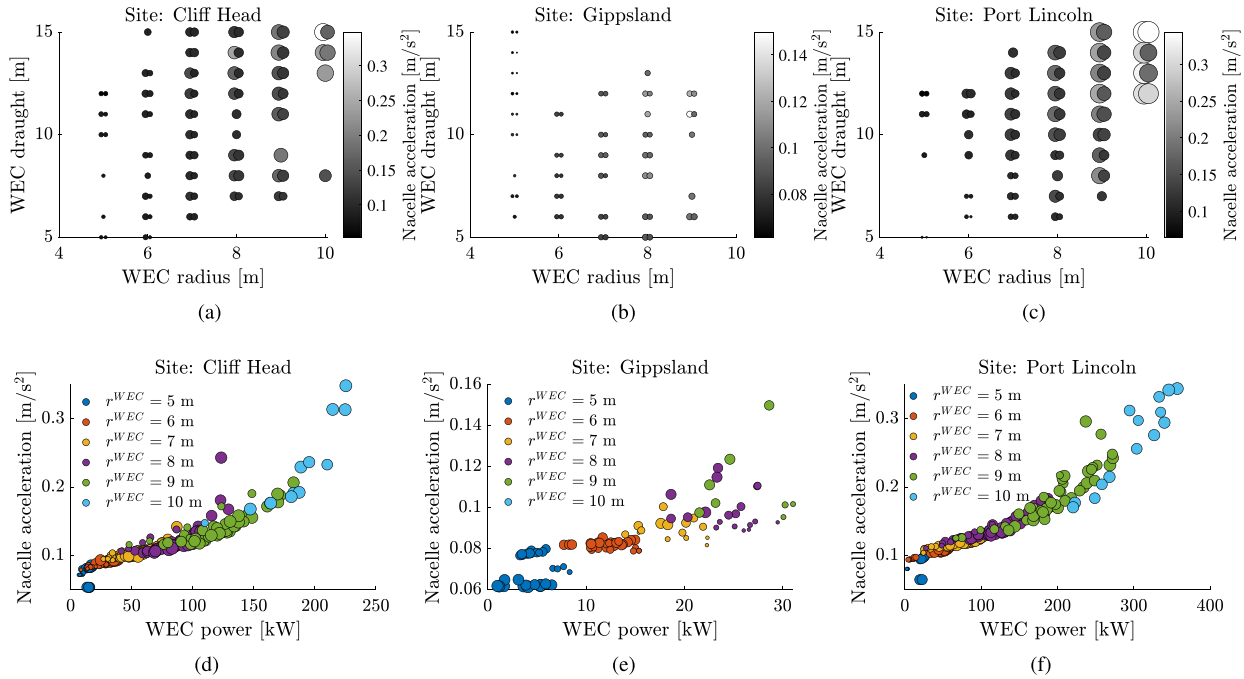

Fig. 25. The dependence of WEC power and wind turbine nacelle acceleration on the WEC radius and draught based on values from Pareto front for the Cliff Head – (a) and (d), Gippsland – (b) and (e), and Port Lincoln – (c) and (f). Refer to Fig. 24 for more details.

- Initially, the effectiveness of the proposed multi-objective optimisation framework is assessed by comparing four sea sites along the South Coast of Australia. However, how well the proposed optimiser performs when applied to other sea sites with different wave scenarios remains uncertain.
- It is also essential to validate the method in real-world scenarios with complex environmental conditions and system constraints to evaluate its effectiveness and applicability.
- Besides, the optimisation objectives primarily focus on maximising the power output of WECs on average and minimising the acceleration of wind turbine nacelles. Nonetheless, it is crucial to extensively consider other important performance metrics, such as

cost-effectiveness, maintenance requirements, and environmental impact, in future research endeavours.
- Furthermore, it can be helpful to thoroughly investigate the scalability of the proposed optimiser for larger-scale hybrid platforms that incorporate multiple floating wind turbines and wave energy converters. The performance and computational efficiency of the method may differ when applied to more intricate and larger-scale systems.
- Lastly, the study concentrates on optimising hybrid wave-wind energy systems for specific deployment sites along the South Coast of Australia. However, exploring the generalisability of the optimisation framework to other geographical locations or

25

different sea conditions can be helpful in order to broaden its applicability to a broader range of scenarios in future studies.

Addressing these limitations would lead to a more exhaustive comprehension of the suggested technique for optimising multiple objectives, amplifying its efficacy in various scenarios, and guaranteeing its applicability in various circumstances and levels of complexity within a system.

6. Conclusions

This paper proposes a fast and effective multi-objective optimisation method (DMOGWA) consisting of a modified swarm intelligence-based optimiser with a chaotic control parameter and an adaptive strategy to update the hyper-parameters for mutation step size with a discretisation technique to speed up the exploitation process. To test the performance of the proposed optimisation framework, a hybrid platform comprised of a semi-submersible floating offshore wind turbine united with three torus-shaped wave energy converters subjected to irregular sea states and turbulent wind. This hybridisation of three WECs with a floating offshore wind turbine makes complex hydrodynamic interactions occur between the floating devices, forming a multi-modal and non-convex optimisation problem. In this regard, two objectives are defined to achieve the highest performance of the hybrid energy model: the average of WECs' power output that should be maximised and reducing the wind turbine nacelle acceleration. Initially, we conducted a comprehensive landscape analysis of the hybrid wave-wind system, examining the model's performance by assessing the feasible range of radius and draught for the WECs, taking into account specific values of K_{pto} and B_{pto}. The optimal range of radius and draught for maximising power output is heavily influenced by the PTO values. Specifically, as the PTO values increase, the optimal radius size transitions from five to ten while the optimal draught range decreases to its minimum value.

According to the computational results, multi-objective swarm and evolutionary algorithms can be effectively utilised to address the multi-objective problem of a hybrid wave-wind energy system. In particular, the best-performing configuration identified in the proposed method (DMOGWA) surpasses the other nine multi-objective optimisation approaches by producing a 135.5% increase in power output (average proximate boost of 36%, 98%, 330%, and 90% in Sydney, Port Lincoln, Gippsland, and Cliff Head, respectively) compared with the standard MOGWO and a 41% reduction in wind turbine nacelle acceleration. DMOGWA showcased its superiority not only in delivering high-quality solutions but also in terms of convergence rate and computational budget savings. The discretisation strategy employed by DMOGWA, which ensures a balanced distribution of PTO parameters within the initial population and adaptive control parameters, played a pivotal role in achieving these remarkable improvements. With its rapid convergence and superior performance, DMOGWA emerges as a promising multi-objective optimisation method for hybrid wave-wind energy systems.

The power enhancement achieved by DMOGWA in the hybrid wave-wind model has far-reaching benefits. It not only contributes to the global efforts of achieving Net zero emissions outlined in the Paris Agreement [93] but also generates significant financial returns. By optimising power generation and maximising revenue potential, DMOGWA plays a pivotal role in driving the transition towards a sustainable energy future while delivering economic advantages for the renewable energy industry.

As a future plan, we aim to explore the scalability of DMOGWA for larger-scale hybrid platforms with multiple floating wind turbines and wave energy converters. Besides, considering additional performance metrics like structural integrity and system reliability would enhance optimisation. Integrating other renewable energy sources and developing a practical implementation plan for hybrid wave-wind energy systems optimised using DMOGWA are also important.

CRediT authorship contribution statement

Mehdi Neshat: Writing – review & editing, Writing – original draft, Visualization, Validation, Software, Methodology, Investigation, Formal analysis, Data curation, Conceptualization. **Nataliia Y. Sergiienko:** Writing – review & editing, Writing – original draft, Visualization, Validation, Software, Resources, Methodology, Investigation, Funding acquisition, Formal analysis, Data curation, Conceptualization. **Meysam Majidi Nezhad:** Writing – review & editing, Investigation, Funding acquisition, Conceptualization. **Leandro S.P. da Silva:** Writing – review & editing, Resources, Investigation, Formal analysis, Conceptualization. **Erfan Amini:** Writing – review & editing, Writing – original draft, Visualization, Investigation, Conceptualization. **Reza Marsooli:** Writing – review & editing, Supervision, Formal analysis, Conceptualization. **Davide Astiaso Garcia:** Writing – review & editing, Supervision, Investigation, Funding acquisition. **Seyedali Mirjalili:** Writing – review & editing, Supervision, Project administration, Methodology, Investigation, Conceptualization.

Declaration of competing interest

The authors declare that they have no known competing financial interests or personal relationships that could have appeared to influence the work reported in this paper.

Data availability

Data will be made available on request.

Acknowledgements

Appendix. Details of multi-objective optimisation methods

A.1. Multi-objective evolutionary algorithm based on decomposition (MOEA/D)

Breaking down multi-objective optimisation problems into individual objectives is a classic approach. This can be done through the use of either a weighted sum of targets or an interval (or norm) of the differentiation vector of targets and a predetermined supreme point in the target space. However, these traditional methods have not been effective in dealing with actual MOO issues and are often unable to find all the possible Pareto solutions [48].

MOEA/D [48], an MOEA developed by Qingfu Zhang and Hui Li in 2007, aims to simplify MOO problems into individual sub-problems with single-objective. This algorithm determines the best solution for each sub-problem by evaluating all of the solutions it finds. MOEA/D works by first creating a population of randomly generated candidates. The solutions are then evaluated on each of the subproblems. Next, The generated candidates should be compared to the Pareto Dominance Frontier, which is a set of keys that are non-dominated by any other solution in the population. The non-dominated solutions are kept, and the rest are discarded. The remaining solutions are then recombined and mutated to generate a new population. This process is iterated until

a satisfactory set of solutions is found. The algorithm also includes a number of strategies for improving the diversity of the Pareto-Optimal Front. These strategies include crowding, niching, and diversity preservation and help to identify a wide range of solutions that cover the entire Pareto-Optimal Front in various real engineering problems and complex energy systems [94].

A.2. Pareto envelope-based selection algorithm II (PESA-II)

PESA-II [44] is an evolutionary algorithm designed for the multi-objective optimisation of complex problems. It is based on the PESA and is used to create a set of solutions that are non-dominated (also known as a Pareto front) and can be used to compare and rank different solutions.

PESA-II works by first randomly generating a set of candidate solutions. Each solution is evaluated against a set of predefined objectives and compared to the existing Pareto ones. If the new solution is not dominated by any of the existing candidates, it is added to the Pareto front. The new solution is then used to generate a new set of candidate solutions, which are evaluated and compared similarly. This algorithm keeps on with it until the desired number of solutions has been developed. The algorithm is relatively simple and can be utilised for any MOO problem. It is fast and efficient and provides a considerable trade-off between accuracy and speed. Additionally, it is robust to noise and can handle non-convex objectives [95].

A.3. Strength pareto evolutionary algorithm II (SPEA-II)

SPEA-II [45] is an improved version of SPEA [96] (an evolutionary MOO algorithm developed by Zitzler and Thiele in 1998). It depends on the idea of Pareto dominance and uses a fitness assignment method to evaluate the strength of each solution in the population. SPEA-II combines a fitness assignment with a fast, non-dominated sorting procedure and an environmental selection based on a 'K-tournament' selection to generate the last group of non-dominated solutions. SPEA-II works by iteratively developing potential solutions and evaluating each according to its fitness. Solutions are then ranked based on their Pareto dominance, and those with the highest Pareto rank are selected for the following replication. This algorithm is iterated till a group of non-dominated candidates is obtained. The main advantages of SPEA-II are its scalability and its ability to handle large numbers of objectives. It is also comparatively simple to develop and has low complexity in terms of computation. Additionally, SPEA-II is able to outperform other evolutionary MOO algorithms in some instances.

A.4. Multi-objective particle swarm optimisation (MOPSO)

MOPSO (Multi-Objective Particle Swarm optimisation) [97,98] is the most well-known swarm-based algorithm that works associated with the principles of PSO. It is distinctively developed to solve multi-objective optimisation problems, which are problems with two or more conflicting objectives. MOPSO is a stochastic algorithm, which means that there is no guarantee of finding a globally optimal candidate. Still, it is capable of finding a solution with high quality within a reasonable runtime.

MOPSO works by creating a swarm of particles, each representing a solution with high potential for the problem. The particles move through the solution space, guided by the fitness of each particle and the fitness of the swarm. At each iteration, the particles update their position based on the best fitness and the best fitness of their neighbours. The particles also use a social element to update their positions, which helps the particles to explore different regions of the solution space. The search stops when a predefined number of iterations have been completed or when the swarm converges on a good solution. The applications of MOPSO are related to a wide range of problems [99], including vehicle routing, scheduling, clustering, image processing, and robotics. Several studies have compared MOPSO with other evolutionary optimisation algorithms, such as GAs and ant colony optimisation, and found that MOPSO outperforms these algorithms in terms of accuracy and efficiency.

A.5. Multi-objective ant lion optimiser (MALO)

Multi-objective Ant Lion optimiser (MALO) [46] is a powerful and efficient multi-objective meta-heuristic optimisation algorithm based on the idea of the ant lion optimisation algorithm (ALO). It was first proposed by Mirjalili and Lewis in 2015. MALO combines the local search abilities of the ant lion with the global search abilities of the multi-objective evolutionary algorithm (MOEA) to discover a group of Pareto optimal solutions for a given problem.

The MALO algorithm is based on two main steps: the first is the Ant Lion optimiser (ALO), which is used for local search, and the second is the Multi-Objective Evolutionary Algorithm (MOEA), which is used for global search. The ALO is used to find the local optima in the search space, while the MOEA is used to find the Pareto optimal solutions. The MALO algorithm has been applied to different optimisation problems, such as feature selection, dynamic economic dispatch, and job shop scheduling. It has been found to outperform other optimisation algorithms such as PSO, GAs, and hybrid PSO+GAs. In addition, MALO has been used in various real-world applications [100], such as parameter optimisation in wind turbine design, optimal design of power transmission lines, and optimal control of water resources.

A.6. Multi-objective dragonfly algorithm (MODA)

MODA [47] is a modified type of the Dragonfly Algorithm with a single objective and is a population-based algorithm that combines the dynamic behaviours of dragonflies in nature in which they look for the most suitable source of food while maintaining a certain distance from other dragonflies.

The MODA algorithm uses a combination of an exploration process, which looks for promising areas of the objective space, and an exploitation process, which focuses on refining the best-found solutions so far. The MODA algorithm also uses an archive of solutions to record the best-performed solutions found so far, and it uses this archive to enhance the effectiveness of the solutions developed by the algorithm. MODA has been successfully utilised for several MOO problems, including feature selection, network design, and portfolio optimisation. It has been evaluated on several benchmark problems [101], including the DTLZ, ZDT and CTP problems. Results show that MODA is competitive with other multi-objective optimisation algorithms, such as NSGA-II and SPEA2.

References

[1] Pfeifer A, Feijoo F, Duić N. Fast energy transition as a best strategy for all? The nash equilibrium of long-term energy planning strategies in coupled power markets. Energy 2023;284:129109.

[2] Karimirad M. Offshore energy structures: for wind power, wave energy and hybrid marine platforms. Springer; 2014.

[3] Amini E, Mehdipour H, Faraggiana E, Golbaz D, Mozaffari S, Bracco G, et al. Optimization of hydraulic power take-off system settings for point absorber wave energy converter. Renew Energy 2022;194:938–54.

[4] de Faria VA, de Queiroz AR, DeCarolis JF. Optimizing offshore renewable portfolios under resource variability. Appl Energy 2022;326:120012.

[5] Cipolletta M, Crivellari A, Moreno VC, Cozzani V. Design of sustainable offshore hybrid energy systems for improved wave energy dispatchability. Appl Energy 2023;347:121410.

[6] Prina MG, Groppi D, Nastasi B, Garcia DA. Bottom-up energy system models applied to sustainable islands. Renew Sustain Energy Rev 2021;152:111625.

[7] Dong X, Li Y, Li D, Cao F, Jiang X, Shi H. A state-of-the-art review of the hybrid wind-wave energy converter. Progr Energy 2022;4(4):042004.

[8] Trinh TT, Pattiaratchi C, Bui T. The contribution of forerunner to storm surges along the Vietnam Coast. J Mar Sci Eng 2020;8(7):508.

[9] Deutch J. Is net zero carbon 2050 possible? Joule 2020;4(11):2237–40.

[10] Cheng F, Luo H, Jenkins JD, Larson ED. The value of low-and negative-carbon fuels in the transition to net-zero emission economies: Lifecycle greenhouse gas emissions and cost assessments across multiple fuel types. Appl Energy 2023;331:120388.

[11] Østergaard PA, Duic N, Noorollahi Y, Mikulcic H, Kalogirou S. Sustainable development using renewable energy technology. Renew Energy 2020;146:2430–7.

[12] Pfeifer A, Guzović Z, Piacentino A, Markovska N, Duić N, Lund H. Cutting-edge science for sustainable development-SDEWES 2022 special issue. Energy 2023;284:129148.

[13] Kemp J, McCowage M, Wang F, et al. Towards net zero: implications for Australia of energy policies in East Asia | Bulletin – September 2021. Reserve Bank of Australia; 2021.

[14] Adams P. Zero greenhouse gas emissions by 2050: What it means for the Australian economy, industries and regions. Centre of Policy Studies Working Paper No. G-324, Victoria University; 2021, p. 3.

[15] Guzovi Z, Duić N, Piacentino A, Markovska N, Mathiesen BV, Lund H, et al. SDEWES science-The path to a sustainable carbon neutral world. Energy 2023;284:1–20.

[16] Zhang Z, Yang H, Zhao Y, Han Z, Zhou D, Zhang J, et al. A novel wake control strategy for a twin-rotor floating wind turbine: Mitigating wake effect. Energy 2024;287:129619.

[17] Gao Q, Ertugrul N, Ding B, Negnevitsky M. Offshore wind, wave and integrated energy conversion systems: A review and future. In: 2020 Australasian universities power engineering conference. IEEE; 2020, p. 1–6.

[18] Robertson A, Jonkman J, Masciola M, Song H, Goupee A, Coulling A, et al. Definition of the semisubmersible floating system for phase II of OC4. Tech. rep., Golden, CO (United States): National Renewable Energy Lab.(NREL); 2014.

[19] Deng Z, Zhang B, Miao Y, Zhao B, Wang Q, Zhang K. Multi-objective optimal design of the wind-wave hybrid platform with the coupling interaction. J Ocean Univ China 2023;22(5):1165–80.

[20] Hu J, Zhou B, Vogel C, Liu P, Willden R, Sun K, et al. Optimal design and performance analysis of a hybrid system combing a floating wind platform and wave energy converters. Appl Energy 2020;269:114998.

[21] Nastasi B, Markovska N, Puksec T, Duić N, Foley A. Techniques and technologies to board on the feasible renewable and sustainable energy systems. Renew Sustain Energy Rev 2023;182:113428.

[22] Kluger JM, Haji MN, Slocum AH. The power balancing benefits of wave energy converters in offshore wind-wave farms with energy storage. Appl Energy 2023;331:120389.

[23] Neshat M, Nezhad MM, Sergiienko NY, Mirjalili S, Piras G, Garcia DA. Wave power forecasting using an effective decomposition-based convolutional Bi-directional model with equilibrium Nelder-Mead optimiser. Energy 2022;256:124623.

[24] Deb K, Pratap A, Agarwal S, Meyarivan T. A fast and elitist multiobjective genetic algorithm: NSGA-II. IEEE Trans Evol Comput 2002;6(2):182–97.

[25] Fadaee M, Radzi M. Multi-objective optimization of a stand-alone hybrid renewable energy system by using evolutionary algorithms: A review. Renew Sustain Energy Rev 2012;16(5):3364–9.

[26] Mirjalili S, Mirjalili SM, Lewis A. Grey wolf optimizer. Adv Eng Softw 2014;69:46–61.

[27] Michailides C, Gao Z, Moan T. Experimental and numerical study of the response of the offshore combined wind/wave energy concept SFC in extreme environmental conditions. Mar Struct 2016;50:35–54.

[28] Ringwood JV, Bacelli G, Fusco F. Energy-maximizing control of wave-energy converters: The development of control system technology to optimize their operation. IEEE Control Syst Mag 2014;34(5):30–55.

[29] Celesti ML, Paduano B, Peña-Sanchez Y, Pasta E, Faedo N, Ringwood J. Design considerations for a hybrid wind-wave platform under energy-maximising control. In: Proceedings of the European wave and tidal energy conference. Vol. 15, 2023.

[30] Coello CA, Lamont GB, Van Veldhuizen DA. Evolutionary algorithms for solving multi-objective problems. Springer Science & Business Media; 2007.

[31] Mirjalili S, Saremi S, Mirjalili SM, Coelho LdS. Multi-objective grey wolf optimizer: a novel algorithm for multi-criterion optimization. Expert Syst Appl 2016;47:106–19.

[32] Letcher T. Future energy: Improved, sustainable, and clean options for our planet. Chem Int–Newsmagazine IUPAC 2008;30(2):20–1.

[33] Falcão AFdO. Wave energy utilization: A review of the technologies. Renew Sustain Energy Rev 2010;14(3):899–918.

[34] Astariz S, Iglesias G. Co-located wind and wave energy farms: Uniformly distributed arrays. Energy 2016;113:497–508.

[35] Korde UA, Lyu J, Robinett III RD, Wilson DG, Bacelli G, Abdelkhalik OO. Constrained near-optimal control of a wave energy converter in three oscillation modes. Appl Ocean Res 2017;69:126–37.

[36] Morteza A, Sadipour M, Fard RS, Taheri S, Ahmadi A. A dagging-based deep learning framework for transmission line flexibility assessment. IET Renew Power Gener 2022.

[37] Liu C, Hu M, Gao W, Chen J, Zeng Y, Wei D, et al. A high-precise model for the hydraulic power take-off of a raft-type wave energy converter. Energy 2021;215:119107.

[38] Coello CAC, Pulido GT, Lechuga MS. Handling multiple objectives with particle swarm optimization. IEEE Trans Evol Comput 2004;8(3):256–79.

[39] Teegavarapu RS, Ferreira AR, Simonovic SP. Fuzzy multiobjective models for optimal operation of a hydropower system. Water Resour Res 2013;49(6):3180–93.

[40] Chen M, Xiao P, Zhou H, Li CB, Zhang X. Fully coupled analysis of an integrated floating wind-wave power generation platform in operational sea-states. Front Energy Res 2022;10:931057.

[41] Tian W, Wang Y, Shi W, Michailides C, Wan L, Chen M. Numerical study of hydrodynamic responses for a combined concept of semisubmersible wind turbine and different layouts of a wave energy converter. Ocean Eng 2023;272:113824.

[42] Zhang X, Li B, Hu Z, Deng J, Xiao P, Chen M. Research on size optimization of wave energy converters based on a floating wind-wave combined power generation platform. Energies 2022;15(22):8681.

[43] Zhang Q, Li H. MOEA/D: A multiobjective evolutionary algorithm based on decomposition. IEEE Trans Evol Comput 2007;11(6):712–31.

[44] Corne DW, Knowles JD, Oates MJ. The Pareto envelope-based selection algorithm for multiobjective optimization. In: Parallel problem solving from nature PPSN VI: 6th international conference Paris, France, September 18–20, 2000 proceedings. Vol. 6. Springer; 2000, p. 839–48.

[45] Zitzler E, Laumanns M, Thiele L. SPEA2: Improving the strength Pareto evolutionary algorithm. TIK-Rep 2001;103.

[46] Mirjalili S, Jangir P, Saremi S. Multi-objective ant lion optimizer: a multi-objective optimization algorithm for solving engineering problems. Appl Intell 2017;46:79–95.

[47] Mirjalili S. Dragonfly algorithm: a new meta-heuristic optimization technique for solving single-objective, discrete, and multi-objective problems. Neural Comput Appl 2016;27:1053–73.

[48] Zhang Q, Li H. MOEA/D: A multiobjective evolutionary algorithm based on decomposition. IEEE Trans Evol Comput 2007;11(6):712–31.

[49] Coello CAC, Lamont GB, Van Veldhuizen DA, et al. Evolutionary algorithms for solving multi-objective problems. vol. 5, Springer; 2007.

[50] Luan C, Michailides C, Gao Z, Moan T. Modeling and analysis of a 5 MW semi-submersible wind turbine combined with three flap-type Wave Energy Converters. In: International conference on offshore mechanics and arctic engineering. Vol. 45547, American Society of Mechanical Engineers; 2014, V09BT09A028.

[51] Luan C. Design and analysis for a steel braceless semi-submersible hull for supporting a 5-MW horizontal axis wind turbine (Ph.D. thesis), NTNU, Norwegian University of Science and Technology; 2018.

[52] Jonkman J, Butterfield S, Musial W, Scott G. Definition of a 5-MW reference wind turbine for offshore system development. Tech. rep., Golden, CO (United States): National Renewable Energy Lab. (NREL); 2009.

[53] Babarit A, Hals J, Kurniawan A, Muliawan M, Moan T, Krokstad J. The NumWEC project. In: Numerical estimation of energy delivery from a selection of wave energy converters–Final report. Starkraft, Centrale Nantes, NTNU; 2011, p. 1–317.

[54] Lee C-H. WAMIT theory manual. Massachusetts Institute of Technology, Department of Ocean Engineering; 1995.

[55] da Silva LS, Cazzolato BS, Sergiienko NY, Ding B. Efficient estimation of the nonlinear aerodynamic loads of floating offshore wind turbines under random waves and wind in frequency domain. J Ocean Eng Mar Energy 2021;1–17.

[56] Jonkman JM, Hayman G, Jonkman B, Damiani R, Murray R. AeroDyn v15 user's guide and theory manual. NREL Draft Report, 2015, p. 46.

[57] on Waves TSC. Final report and recommendations to the 23rd ITTC. In: Proceedings of the 23rd international towing tank conference. Vol. II, 2002, p. 505–736.

[58] Burton T, Sharpe D, Jenkins N, Bossanyi E. Wind energy handbook. vol. 2, Wiley Online Library; 2001.

[59] Van Der Tempel J, Diepeveen N, De Vries W, Salzmann DC. Offshore environmental loads and wind turbine design: impact of wind, wave, currents and ice. In: Wind energy systems. Elsevier; 2011, p. 463–78.

[60] da Silva LSP, de Oliveira M, Cazzolato B, Sergiienko N, Amaral G, Ding B. Statistical linearisation of a nonlinear floating offshore wind turbine under random waves and winds. Ocean Eng 2022;261:112033.

[61] Holmes JD, Bekele S. Wind loading of structures. vol. 11, London: SPON Press; 2001.

[62] Sø rensen P, Hansen AD, Rosas PAC. Wind models for simulation of power fluctuations from wind farms. J Wind Eng Ind Aerodyn 2002;90(12–15):1381–402.

[63] Wind energy generation systems - Part 3-2: Design requirements for floating offshore wind turbines. Standard IEC 61400-3-2, Geneva, Switzerland: International Electrotechnical Commission; 2019.

[64] Marine energy - Wave, tidal and other water current converters - Part 2: Marine energy systems - Design requirements. Standard IEC 62600-2, Geneva, Switzerland: International Electrotechnical Commission; 2019.

[65] da Silva LSP, Sergiienko NY, Pesce CP, Ding B, Cazzolato B, Morishita HM. Stochastic analysis of nonlinear wave energy converters via statistical linearization. Appl Ocean Res 2020;95:102023.

[66] Sclavounos P, Tracy C, Lee S. Floating offshore wind turbines: Responses in a seastate Pareto optimal designs and economic assessment. In: International conference on offshore mechanics and arctic engineering. Vol. 48234, 2008, p. 31–41.

[67] Wind turbine generator systems-part 1: Safety requirements. Standard IEC 61400-1, Geneva, Switzerland: International Electrotechnical Commission; 1991.

[68] Li M, Yao X. Quality evaluation of solution sets in multiobjective optimisation: A survey. ACM Comput Surv 2019;52(2):1–38.

[69] Coello CAC. Theoretical and numerical constraint-handling techniques used with evolutionary algorithms: a survey of the state of the art. Comput Methods Appl Mech Engrg 2002;191(11–12):1245–87.

[70] Hu Z, Yang J, Sun H, Wei L, Zhao Z. An improved multi-objective evolutionary algorithm based on environmental and history information. Neurocomputing 2017;222:170–82.

[71] Shadmani A, Nikoo MR, Etri T, Gandomi AH. A multi-objective approach for location and layout optimization of wave energy converters. Appl Energy 2023;347:121397.

[72] Deb K. Multi-objective optimisation using evolutionary algorithms: an introduction. Springer; 2011.

[73] Coello CAC. Multi-objective optimization. In: Handbook of heuristics. Springer; 2018, p. 177–204.

[74] Qian J, Sun X, Zhong X, Zeng J, Xu F, Zhou T, et al. Multi-objective optimization design of the wind-to-heat system blades based on the Particle Swarm Optimization algorithm. Appl Energy 2024;355:122186.

[75] Medhane DV, Sangaiah AK. Search space-based multi-objective optimization evolutionary algorithm. Comput Electr Eng 2017;58:126–43.

[76] Liu H, Li Y, Duan Z, Chen C. A review on multi-objective optimization framework in wind energy forecasting techniques and applications. Energy Convers Manage 2020;224:113324.

[77] Liu L, Zhai R, Hu Y. Multi-objective optimization with advanced exergy analysis of a wind-solar-hydrogen multi-energy supply system. Appl Energy 2023;348:121512.

[78] Srinivas N, Deb K. Muiltiobjective optimization using nondominated sorting in genetic algorithms. Evol Comput 1994;2(3):221–48.

[79] Deb K, Jain H. An evolutionary many-objective optimization algorithm using reference-point-based nondominated sorting approach, part I: solving problems with box constraints. IEEE Trans Evol Comput 2013;18(4):577–601.

[80] Niveditha N, Singaravel MR. Optimal sizing of hybrid PV–wind–battery storage system for net zero energy buildings to reduce grid burden. Appl Energy 2022;324:119713.

[81] Zou D, Gong D, Ouyang H. A non-dominated sorting genetic approach using elite crossover for the combined cooling, heating, and power system with three energy storages. Appl Energy 2023;329:120227.

[82] Chen J, Huang S, Shahabi L. Economic and environmental operation of power systems including combined cooling, heating, power and energy storage resources using developed multi-objective grey wolf algorithm. Appl Energy 2021;298:117257.

[83] Makhadmeh SN, Alomari OA, Mirjalili S, Al-Betar MA, Elnagar A. Recent advances in multi-objective grey wolf optimizer, its versions and applications. Neural Comput Appl 2022;34(22):19723–49.

[84] Liu J, Yang Z, Li D. A multiple search strategies based grey wolf optimizer for solving multi-objective optimization problems. Expert Syst Appl 2020;145:113134.

[85] Neshat M, Alexander B, Wagner M. A hybrid cooperative co-evolution algorithm framework for optimising power take off and placements of wave energy converters. Inform Sci 2020;534:218–44.

[86] Deb K, Agrawal S, Pratap A, Meyarivan T. A fast elitist non-dominated sorting genetic algorithm for multi-objective optimization: NSGA-II. In: Parallel problem solving from nature PPSN VI: 6th international conference Paris, France, September 18–20, 2000 proceedings. Vol. 6. Springer; 2000, p. 849–58.

[87] Zheng W, Doerr B. Better approximation guarantees for the NSGA-II by using the current crowding distance. In: Proceedings of the genetic and evolutionary computation conference. 2022, p. 611–9.

[88] Coello CAC, Pulido GT, Lechuga MS. Handling multiple objectives with particle swarm optimization. IEEE Trans Evol Comput 2004;8(3):256–79.

[89] Knowles JD, Corne DW. Approximating the nondominated front using the Pareto archived evolution strategy. Evol Comput 2000;8(2):149–72.

[90] Malan KM, Ochoa G. Recent advances in landscape analysis for optimisation and learning. In: GECCO companion. 2021, p. 899–917.

[91] Guerreiro AP, Fonseca CM, Paquete L. The hypervolume indicator: Computational problems and algorithms. ACM Comput Surv 2021;54(6):1–42.

[92] Mirjalili S, Lewis A. Novel performance metrics for robust multi-objective optimization algorithms. Swarm Evol Comput 2015;21:1–23.

[93] Guzović Z, Duić N, Piacentino A, Markovska N, Mathiesen BV, Lund H. Paving the way for the Paris agreement: Contributions of SDEWES science. Energy 2023;263:125617.

[94] Zou D, Gong D, Ouyang H. The dynamic economic emission dispatch of the combined heat and power system integrated with a wind farm and a photovoltaic plant. Appl Energy 2023;351:121890.

[95] Tian Y, Si L, Zhang X, Cheng R, He C, Tan KC, et al. Evolutionary large-scale multi-objective optimization: A survey. ACM Comput Surv 2021;54(8):1–34.

[96] Zitzler E, Thiele L. An evolutionary algorithm for multiobjective optimization: The strength pareto approach. TIK-Rep 1998;43.

[97] Coello CC, Lechuga MS. MOPSO: A proposal for multiple objective particle swarm optimization. In: Proceedings of the 2002 congress on evolutionary computation. Vol. 2, IEEE; 2002, p. 1051–6.

[98] Pulido GT, Coello Coello CA. Using clustering techniques to improve the performance of a multi-objective particle swarm optimizer. In: Genetic and evolutionary computation conference. Springer; 2004, p. 225–37.

[99] Lalwani S, Singhal S, Kumar R, Gupta N. A comprehensive survey: Applications of multi-objective particle swarm optimization (MOPSO) algorithm. Trans Combinat 2013;2(1):39–101.

[100] Wang J, Du P, Lu H, Yang W, Niu T. An improved grey model optimized by multi-objective ant lion optimization algorithm for annual electricity consumption forecasting. Appl Soft Comput 2018;72:321–37.

[101] Tian H, Yuan C, Li K. Robust optimization of the continuous annealing process based on a novel Multi-Objective Dragonfly Algorithm. Eng Appl Artif Intell 2021;106:104448.